REVIEW

Check for updates

A study of contemporary progress relating to COF materials for CO_2 capture and fixation reactions

Robius Sani,† Tusar Kanto Dey,† Mainak Sarkar, Priyanka Basu and Sk. Manirul Islam [ID] *

Global warming is a great threat to the very survival of our planet. Among the different greenhouse gases, carbon dioxide is pre-eminently responsible for the occurrence of global warming. Therefore, to overcome this problem, covalent organic frameworks (COFs) have been developed as a new class of multifunctional crystalline organic catalyst constructed from organic monomers *via* robust covalent bonds. COF materials could be used for the chemical fixation of CO_2 with different organic molecules to synthesize various valuable chemicals. The specific surface area of the covalent organic framework plays a vital role in the catalytic performance of a COF during chemical conversion involving CO_2. The incorporation of various metals, such as Pd, Cu, Ag, and Ni, into a COF material can enhance its catalytic efficacy during carbon dioxide fixation reactions. Basically, a Schiff base reaction between an amine and aldehyde can result in the formation of a cyclic COF, *e.g.*, TFPB–TAPB-COF, TFPA–TAPB-COF, BTMA–TAPA-COF, and TFPA–TAPA-COF, as reported by Donglin Jiang *et al.* Different kinds of valuable chemicals have been synthesized using these COFs, such as cyclic carbonates, oxazolidinones, *N*-formylated products, formic acid, formaldehyde, and methanol. In this review paper, we present recent advances in this area, including the development of various types of COFs and their application as catalysts for different types of CO_2 fixation reactions. Herein we mainly describe synthesis schemes, some important characterization information (specifically N_2-BET and XRD data), and examples of CO_2 fixation reactions performed using these previously reported COFs. The excellent CO_2 absorption capacities of COFs make them tremendous catalysts for CO_2 conversion, and they can act as CO_2 storage materials.

Department of Chemistry, University of Kalyani, Kalyani, Nadia 741235, West Bengal, India. E-mail: manir65@rediffmail.com; Fax: +91-33-2582-8282; Tel: +91-33-2582-8750

† These authors contributed equally.

1. Introduction

The continuous emission of greenhouse gases is causing global warming, resulting in a constant increase in the earth's temperature. Almost 60% of global warming is caused by carbon

Robius Sani is currently pursuing his PhD under the supervision of Prof. Sk. Manirul Islam from the University of Kalyani. He received his BSc and MSc degrees in Chemistry from the University of Kalyani. His current research is focused on the development of porous heterogeneous catalysts for the synthesis of value-added chemicals.
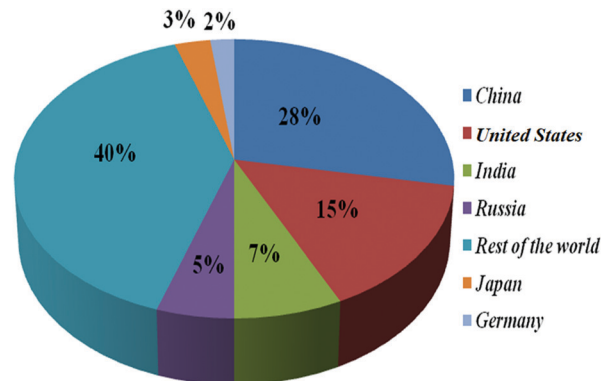
Robius Sani

Tusar Kanto Dey obtained his MSc degree from the Department of Chemistry, University of Kalyani. He received his PhD degree in the year 2022 under the supervision of Prof. Sk. Manirul Islam from University of Kalyani. His research work is based on designing polymer-supported heterogeneous catalysts for in situ carbonylation reactions and the chemical fixation of CO_2 and CO.

Tusar Kanto Dey

dioxide gas. 30 GT of carbon dioxide gas is emitted per year due to fossil fuel consumption, increasing the CO_2 gas concentration in the atmosphere to 400 ppm, a drastic elevation over normal levels (300 ppm). The International Energy Agency, in 2012, predicted that the global temperature will have increased by 2 °C by 2100 and the CO_2 concentration will have reached up to 500 ppm. A major concern of the present era is the increased concentration of carbon dioxide in the earth's atmosphere due to the incineration of fossil fuels. This enhanced amount of CO_2 has a deadly impact on our surroundings.[1] It also affects the global environment, making it hotter. The global temperature is increasing by 0.2 °C per decade, causing global climate change and the melting of icebergs. As a result, sea levels are also increasing every decade due to this melting. Fig. 1 shows the CO_2 emission levels in 2020 from different countries.

To save the environment, there is a very urgent need to decrease CO_2 levels immediately, and atmospheric CO_2 can be used to produce many valuable chemicals *via* different techniques.[2] Researchers have found different protocols for the chemical fixation of carbon dioxide into different organic

Country	Amount of CO_2 emission
China	10.06 GT
United states	5.41 GT
India	2.65 GT
Russia	1.71 GT
Japan	1.16 GT
Germany	0.75 GT
GT = metric gigatons Figures represent fuel consumption only	

Fig. 1 CO_2 emissions in 2020 from different countries.

substrates.[2,3] However, the chemical fixation of carbon dioxide is thermodynamically unfavorable.[3] The chemical fixation of CO_2 into organic substrates is very challenging due to the high activation energy. Thermodynamically, the Gibbs free energy changes in CO_2 fixation reactions are positive, making the chemical fixation of CO_2 thermodynamically unfavorable. For this reason, CO_2 fixation reactions are generally performed with

Mainak Sarkar received his MSc degree (2020) in chemistry from University of Kalyani. He is currently working as a PhD student under the guidance of Prof. Sk. Manirul Islam at University of Kalyani. His research focuses on the development of new COFs for CO_2 capture and the synthesis of value-added chemicals.

Mainak Sarkar

Priyanka Basu obtained her MSc degree from the University of Kalyani in 2014, and she is now working toward her PhD degree under the supervision of Prof. Sk. Manirul Islam from University of Kalyani. Her research work is focused on the development of polymer and oxide supported porous catalysts and their application in the synthesis of fine chemicals, along with CO_2 fixation and carbonylation reactions.

Priyanka Basu

Prof. Sk. Manirul Islam obtained his PhD degree from the Indian Institute of Technology Kharagpur in 1999 and carried out post-doctoral research at the State University of New York, USA from 2000–2001. At present, he is a Professor of Chemistry at the University of Kalyani, West Bengal, India. The present direction of his research is the design and synthesis of functionalized porous materials, COFs, MOFs, and POPs, and their catalytic application in CO_2

Sk. Manirul Islam

fixation to form value-added chemicals, the in situ transformation of CO, the catalytic conversion of CO into value-added chemicals, biofuel synthesis, C–C/CN bond formation reactions, multicomponent coupling reactions, etc.

reagents that have high negative Gibbs free energy changes. To overcome the high activation energy, high CO_2 pressures, elevated reaction temperatures, and prolonged reaction times are required. These reaction conditions are not profitable for the industrial large-scale synthesis of valued-added products *via* CO_2 fixation reactions. These exertions can be overruled *via* designing a suitable catalytic system for the chemical conversion of CO_2. CO_2 is a non-toxic, renewable, inexpensive, and abundant raw C1 feedstock, and it can act as a C1 building block for the synthesis of various valuable chemicals with added economic value, such as carbonates, carbamates, urea, *etc.*[4–7] Different types of catalysts can be designed for this purpose, like porous organic polymers (POPs), metal organic frameworks (MOFs), covalent organic frameworks (COFs), oxide-based compounds, ionic liquids, *etc.*[4–9] The designed catalysts should be selective, stable, easily recoverable from the reaction medium, durable, and highly efficient for industrial applications. Lots of catalytic systems have been reported for the conversion of CO_2 to value-added products, but at present they are unsuitable due to the need for harsh reaction conditions, facing issues like high reaction pressures, difficulties in recoverability, high production costs, *etc.* In the present situation, COFs are outstanding materials for CO_2 storage and conversion due to their exceptional structures and porosity.[7] These materials can be utilized effectively for different types of CO_2 fixation reactions.

Covalent organic frameworks are an excellent class of crystalline porous polymer with two-dimensional or three-dimensional arrangements in an ordered manner, and they are formed from repeating organic precursors. They have excellent surface areas, periodic frameworks, suitable densities, and tuneable functional groups.[8] The extraordinary structural characteristics of COFs make them outstanding versatile materials for use in heterogeneous catalysis, gas adsorption and storage, sensors, and optoelectronics.[9] In 2005, Omar M. Yaghi and Adiren P. Cote first reported a 2-D COF at the University of Michigan.[10] They used phenyl diboronic acid and hexahydroxytriphenylene as building blocks for the synthesis of their COF. Their synthesized COF has excellent thermal stability up to 600 °C, a high surface area, and high porosity. The most interesting aspect of COFs is that their structures can be designed according to the application requirements, and they have tuneable porosity and surface areas, making them exceptional crystalline solids *versus* other available solid crystalline materials.[11] Depending on the building blocks used, COFs can be classified mainly into three categories: triazine-supported, imine-supported, and boron-containing COFs.[12] Covalent triazine frameworks are usually synthesized from repeating nitrile building blocks and these COFs have an inferior crystalline

nature, although they have outstanding thermal stability and chemically inertness.[13] Imine-based COFs can be synthesized in two ways: either *via* Schiff base formation between an aldehyde and a ketone[14] or *via* condensation between an aldehyde and a hydrazide.[15] These imine-supported COFs are highly stable in a variety of solvents and many metals can be grafted onto these COFs in chelate form because of their nitrogen-enriched structures.[16]

The adsorption of CO_2 in a COF depends on some factors, like the building blocks or framework of the COF, the type of linkages between the repeating units, and the porosity type. It has been observed that COFs having triarylamine in their structures are excellent CO_2 storage materials, and the adsorption efficiency increases with an increase in the triarylamine content. Donglin Jiang *et al.* recently reported four imine-linked COFs, TFPB–TAPB-COF, TFPA–TAPB-COF, BTMA–TAPA-COF, and TFPA–TAPA-COF, with similar hexagonal structures and almost the same porosity.[17] They used tris(4-aminophenyl)-amine and tris(4-formylphenyl)amine as triarylamine blocks and 1,3,5-tris(4-formylphenyl)benzene, 1,3,5-tris(4-aminophenyl)-benzene, and 4,4′,4″-boranetriyltris(2,3,5,6-tetramethylbenz-aldehyde) as non-triarylamine building blocks. The CO_2 uptake capacities of the four types of COF are presented in Table 1. It was observed that TFPB–TAPB-COF acts as a very poor material for CO_2 adsorption due to the lack of triarylamine units. TFPA–TAPB-COF contains three triarylamine units in its framework, and it showed a 2.75-fold increase at 298 K and a 3-fold increase at 273 K in terms of the CO_2 adsorption capacity compared with TFPB–TAPB-COF, which does not have any triarylamine units. BTMA–TAPA-COF also contains the same number of triarylamine units (three), but due to the presence of boron in its framework it showed better CO_2 adsorption capacity. The maximum CO_2 adsorption capacity was shown by TFPA–TAPA-COF, which contains six triarylamine units in its framework, and it shows an almost 4.34-fold increase at 298 K and a 5.25-fold increase at 273 K in terms of CO_2 adsorption capabilities compared with TFPB–TAPB-COF, which does not contain any triarylamine units. Therefore, increasing the number of triarylamine units increases the CO_2 adsorption capabilities, and this type of COF can be used as an efficient catalyst for CO_2 fixation reactions.

Another important fact about COFs is that the presence of positively charged pores can effectively enhance the CO_2 intake capacity. Ionic-liquid-immobilized $[Et_4NBr]_{50\%}$-Py-COF can take up 164.6 mg g^{-1} CO_2 at 0 °C under atmospheric pressure.[18] Other functional groups like azo[19] and carboxylic acid[20] groups can also improve the CO_2 intake capacity.

Through this review article, we try to present recent advances relating to different COF materials for CO_2 fixation

Table 1 CO_2 uptake capacities of different COFs

COF	Surface area (m^2 g^{-1})	Pore volume (cm^3 g^{-1})	Average pore size (nm)	CO_2 uptake capacity (wt%)
TFPB–TAPB-COF	410	0.19	1.91	1.2 at 298 K and 2.0 at 273 K
TFPA–TAPB-COF	540	0.25	1.72	3.3 at 298 K and 6.1 at 273 K
BTMA–TAPA-COF	630	0.32	1.59	4.5 at 298 K and 8.4 at 273 K
TFPA–TAPA-COF	660	0.32	1.59	5.2 at 298 and 10.5 at 273 K

reactions producing cyclic carbonates, carbamates, oxazolidinones, N-formylated products, etc. We have tried to detail the structural features and some important characterization experiment results that will definitely help provide a better understanding of COF materials and the CO_2 fixation reactions that are performed by the reported COFs.

2. Different COF-catalyzed CO_2 fixation reactions

2.1 N-Formylation of aromatic amines

In 2016, Yanan Gao et al. presented the immobilization of the ionic liquid $[Et_4NBr]^+Br^-$ inside the framework of a COF. After synthesizing an ionic-liquid COF named $[Et_4NBr]_{50\%}$-Py-COF, it was employed in the transformation of carbon dioxide into valuable formamides under mild reaction conditions.[18] Different molar ratios of 2,5-dihydroxyterephthalaldehyde and 1,4-phthalaldehyde were used along with 1,3,6,8-tetraphenyl-1,8-dihydro-pyrene to synthesize COFs, referred to as $[HO]_{X\%}$-Py-COFs, and after immobilizing the ionic liquid $[Et_4NBr]^+Br^-$, they acquired $[Et_4NBr]_{X\%}$-Py-COFs via a Williamson ether reaction (Scheme 1).[18] The authors found the PXRD patterns of $[HO]_{0\%}$-Py-COF, $[HO]_{100\%}$-Py-COF, and all other COFs with different 'X' values to be same, with peaks at 3.72, 5.23, 4.74, 8.67, 11.29, 15.17, and 23.69 degrees due to the (110), (020), (220), (030), (040), (060), and (001) planes, respectively (Fig. 2). They followed several protocols to confirm the formation of $[Et_4NBr]_{50\%}$-Py-COFs, studying the ion density. The bromide content was determined with the help of ion chromatography (4.6% and 8.9% for X = 25 and 50, respectively). The research group showed the porous nature of the COFs based on N_2 adsorption isotherms at 77 K. They observed that $[HO]_{X\%}$-Py-COFs showed type-IV isotherms, which are characteristic of
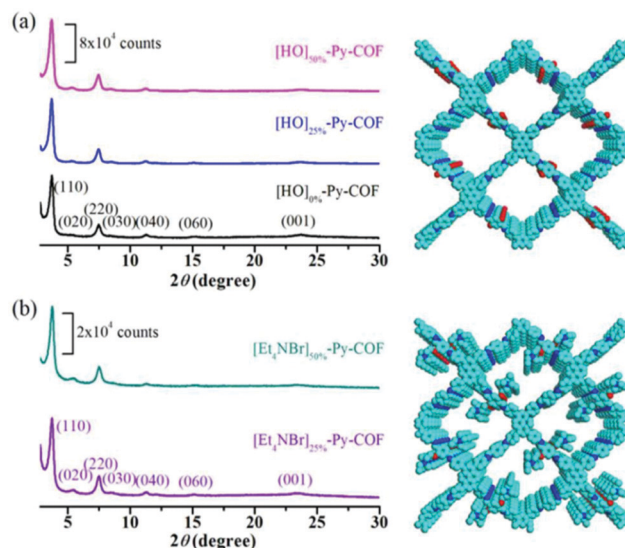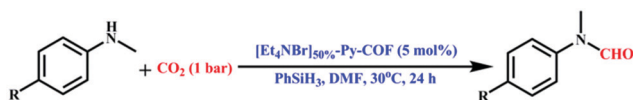

Fig. 2 Powder X-ray diffraction analysis of (a) $[HO]_{X\%}$-Py-COFs (where X is 0, 25, and 50) and (b) $[Et_4NBr]_{X\%}$-Py-COFs (where X is 25 and 50). Top views of $[HO]_{50\%}$-Py-COF and $[Et_4NBr]_{X\%}$-Py-COF (X = 50) are given in the right-side panels. Reproduced with permission from ref. 18; copyright: 2016, Chemical Communications.
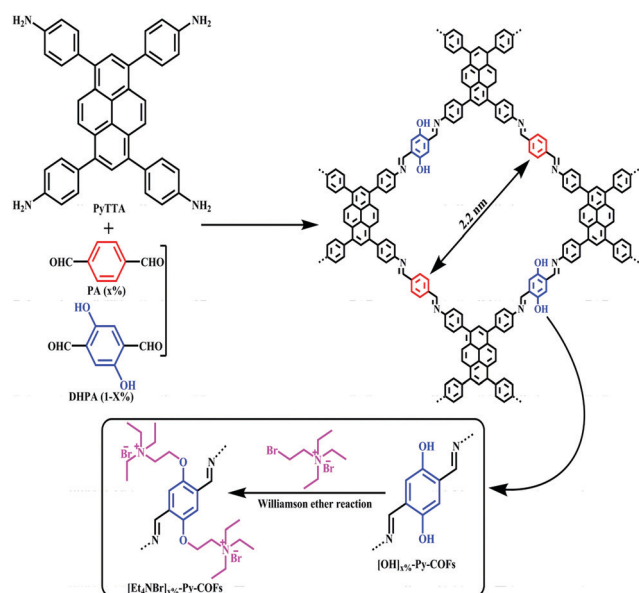

Scheme 2 The synthesis of N-formylated products using $[Et_4NBr]_{X\%}$-Py-COFs.

mesoscopic materials. The N_2-adsorption study showed that the surface coverage, pore volume, and pore size became smaller when the ionic liquid was introduced in the case of $[HO]_{X\%}$-Py-COFs.
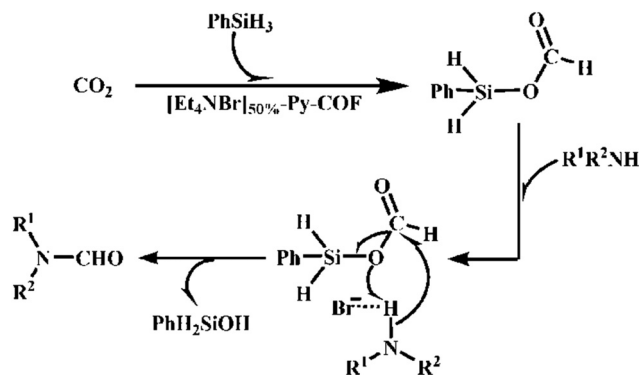
The Y. Gao group performed N-formylation reactions involving various amines efficiently using $[Et_4NBr]_{X\%}$-Py-COFs as immiscible catalysts. Primarily, they executed the N-formylation of N-methylaniline under 1 bar CO_2 pressure and at 30 °C taking DMF as the solvent and phenyl silane as a source of hydrogen (Scheme 2). The Gao research group acquired N-formylated N-methylaniline as the only product with an excellent yield of 94%. They also applied $[HO]_{50\%}$-Py-COF as the catalyst and observed a poor catalytic outcome, gaining a yield of only 32%. This research group studied different kinds of N-methylaniline substrates with electron-withdrawing and donating substituents, and they also responded in a similar way in the N-formylation reaction. A plausible reaction mechanism involving phenyl silane was also demonstrated (Scheme 3).

2.2 Cycloaddition reactions between CO_2 and substituted epoxides

Recently, Ramanathan Vaidhyanathan and his team developed a resorcinol-phenylenediamine-based COF loaded with Ag nanoparticles, which was designated as IISERP-COF15 and applied to the chemical fixation of CO_2.[21] They prepared

Scheme 1 The fabrication of $[HO]_{X\%}$-Py-COFs along with $[Et_4NBr]_{X\%}$-Py-COFs.

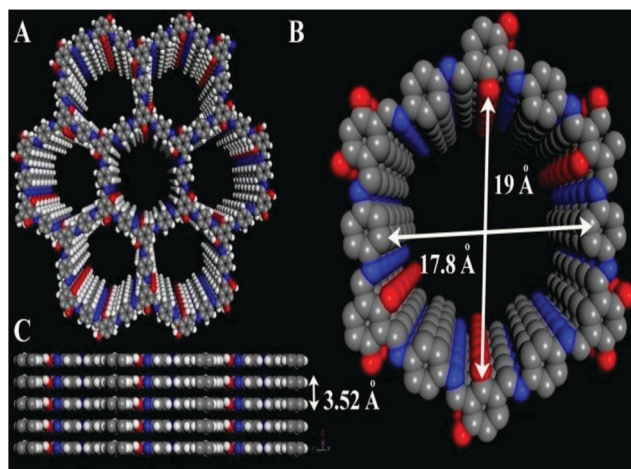**Scheme 3** A plausible mechanism supporting *N*-formylation.

Fig. 3 The 3D structure of Ag@COF. Reproduced with permission from ref. 21; copyright: 2019, Chemistry An Asian Journal.
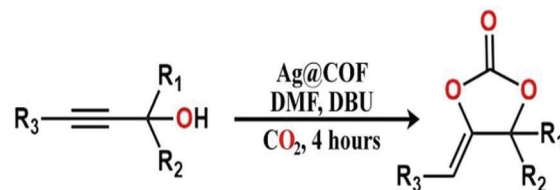
IISERP-COF15 *via* treating triformyl-resorcinol and phenylene-diamine in a dioxane and mesitylene mixture at a ratio of 1 : 1 (v/v) under solvothermal conditions, and then the silver nano-particles were encapsulated into the COF (Fig. 3).

The research group carried out numerous characterization studies to establish the structure of the COF. *Via* PXRD analysis they identified that the COF has a crystalline structure, having a uniform pore size of 14 Å. The PXRD peaks of the Ag-nanoparticle-loaded COF appeared at 2θ values of $38.1°$, $44.1°$, $64.1°$, and $77.1°$ for the (111), (200), (220), and (311) planes, respectively, due to the Ag nanoparticles, and it also showed the characteristic low-angle peaks of the COF. In addition, thermogravimetric analysis showed that the COF is stable up to 300 °C and that the COF can retain its crystalline structure up to 250 °C. Through a N_2 adsorption–desorption study the research group determined that IISERP-COF-15 has significantly high BET and Langmuir surface areas of 1230 and 1540 $m^2\ g^{-1}$, respectively. They observed that the volume of the COF pores is 0.6332 $cm^3\ g^{-1}$ and their size is 12 Å with the help of non-local density functional theory (NLDFT) (Fig. 4).

Dr Vaidhyanathan and his research team treated 1,8-diaza-bicyclo[5.4.0]undec-7-ene (DBU) and propargyl alcohol under a
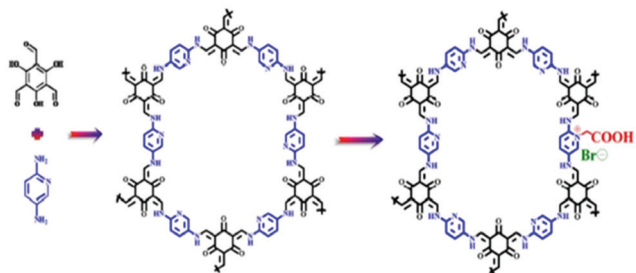

Fig. 4 (A) The N_2 adsorption isotherm of IISERP-COF–15. (B) The PXRD pattern of the COF. (C) The PXRD pattern of Ag@COF. Reproduced with permission from ref. 21; copyright: 2019, Chemistry An Asian Journal.

Scheme 4 A synthetic diagram of the formation of cyclic carbonates. Reproduced with permission from ref. 21; copyright: 2019, Chemistry An Asian Journal.

CO_2 atmosphere using Ag@COF as the catalyst and DMF as the solvent for 4 h and obtained a cyclic carbonate yield of 90% and a TON greater than 150 (Scheme 4). The research group claimed that the microporous structure and high surface area of Ag@COF are highly effective for the conversion of CO_2 into cyclic carbonates, and the COF can be reused up to five times with only a minute change in its catalytic activity.

Miao Du *et al.* and his team designed a metal-free bi-functional COF catalyst for coupling CO_2 with epoxides to form cyclic carbonates under gentle reaction conditions and they designated the catalyst as TpPa-Py-Br⁻-COF (Scheme 5). This unique bi-functional COF has both active nucleophilic sites and Brønsted acid catalytic sites.[22] The research group synthesized TpPa-Py COF *via* treating 2,4,6-trihydroxybenzene-1,3,5-tri-carbaldehyde, 2,5-diaminopyridine, 1,4-dioxane, mesitylene, and aqueous acetic acid (6 M) in a sealed Pyrex pressure tube at 120 °C for three days. After that, they treated COF-TpPa-Py with a solution of saturated Br–CH_2COOH under a N_2 atmosphere for one day at 70 °C and finally obtained TpPa-Py-Br⁻-COF. The Br⁻

Scheme 5 The synthesis of TpPa-Py-Br$^-$-COF. Reproduced with permission from ref. 22; copyright: 2020, ChemCatChem.
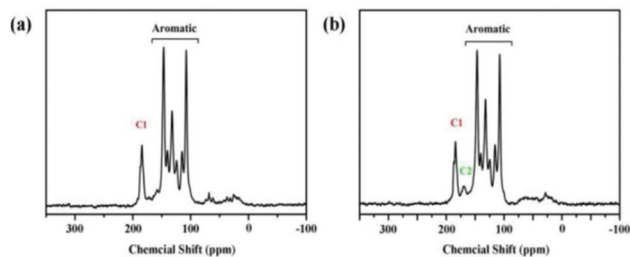

Fig. 5 (a) The solid-state ^{13}C-NMR spectrum of TpPa-Py-COF. (b) The solid-state ^{13}C-NMR spectrum of TpPa-Py-Br$^-$-COF. Reproduced with permission from ref. 22; copyright: 2020, ChemCatChem.

content in TpPa-Py-Br$^-$-COF is 1.25 wt%, with 0.149 mmol g^{-1} total acid sites.

The research group confirmed the successful formation of TpPa-Py-Br$^-$-COF *via* solid-state ^{13}C-NMR (Fig. 5), FT-IR and PXRD (Fig. 6), and XPS analysis. The FT-IR spectrum confirms the successful formation of TpPa-Py-Br$^-$-COF *via* the binding of BrCH$_2$COOH to TpPa-Py-COF and it also confirms the presence of carboxylic groups in the COF structure. The PXRD patterns of TpPa-Py-COF and TpPa-Py-Br$^-$-COF do not show much difference, revealing that there are no ordered long-range structures.

N$_2$ absorption–desorption studies confirm the permanent porous nature of TpPa-Py-COF and TpPa-Py-Br$^-$-COF (Fig. 7). The total calculated BET surface areas of TpPa-Py-COF and TpPa-Py-Br$^-$-COF are found to be 514 m^2 g^{-1} and 113 m^2 g^{-1}, respectively. The calculated P/P_0 values range from 0.054099 to 0.295057 for TpPa-Py-COF, while for TpPa-Py-Br$^-$-COF these values lie between 0.084401 and 0.294829. From thermogravimetric
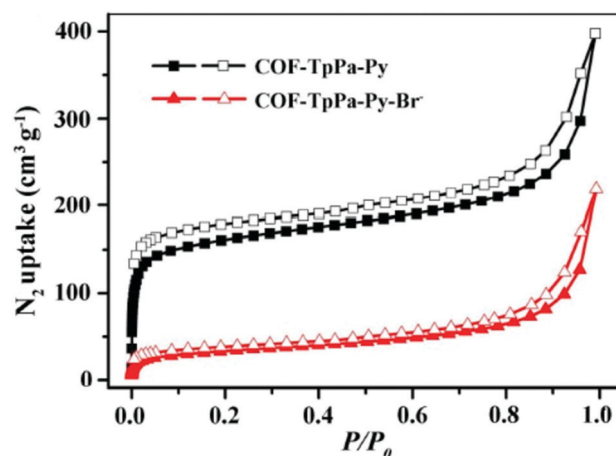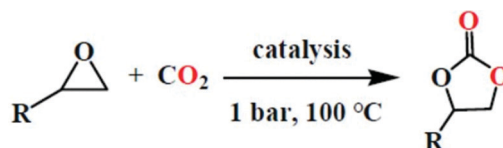

Fig. 6 FT-IR and PXRD patterns of TpPa-Py-Br$^-$-COF. Reproduced with permission from ref. 22; copyright: 2020, ChemCatChem.

Fig. 7 The N$_2$ adsorption isotherm of TpPa-Py-Br$^-$-COF. Reproduced with permission from ref. 22; copyright: 2020, ChemCatChem.

Scheme 6 The synthesis scheme for cycloaddition involving CO$_2$. Reproduced with permission from ref. 22; copyright: 2020, ChemCatChem.

analysis, it was established that TpPa-Py-COF and TpPa-Py-Br$^-$-COF are stable up to 450 °C.

Miao Du *et al.* and his research group used different substrates for CO$_2$ cycloaddition reactions (Scheme 6). They treated epichlorohydrin under a CO$_2$ atmosphere at 100 °C using TpPa-Py-Br$^-$-COF as a catalyst and achieved a 99% cyclic carbonate yield. Their experimental observations showed that the yield was reduced to 1% from 99% upon lowering the temperature to 40 °C from 100 °C. They determined that the cyclic carbonate yield decreased from 99% to less than 1% *via* the non-catalytic path. The group also showed that this heterogeneous porous bi-functional COF can be reused five times without any significant reduction in catalytic activity. Therefore, all these experimental observations confirm that COF-TpPa-Py-Br$^-$ is an excellent catalyst for CO$_2$ cycloaddition reactions involving epoxides.

Another interesting material was reported by H. Wang *et al.* in the form of a metallo-porphin-based two-dimensional COF and this was applied to the preparation of cyclic carbonates *via* CO$_2$ fixation reactions.[23] The covalent organic framework they synthesized was denoted as COF-366-Zn, and this was used for the formation of 4-ethyl-[1,3]dioxolan-2-one, having activity of ~99.2% under gentle reaction conditions. In this context, they showed that embedding Zn and Co metal into 2-dimensional COFs, *i.e.*, COF-366 and COF-SQ, resulted in marvelous catalytic activity for the transformation of CO$_2$ to cyclic carbonates. They processed COF-366 *via* applying a condensation method involving tetra-(amidogenphenyl)-porphine and 1,4-benzenedi-carboxaldehyde. For the synthesis of COF-SQ, a squaric acid
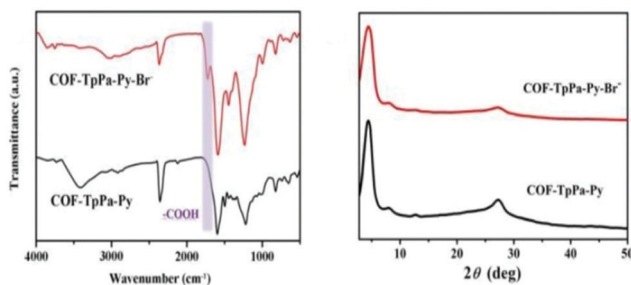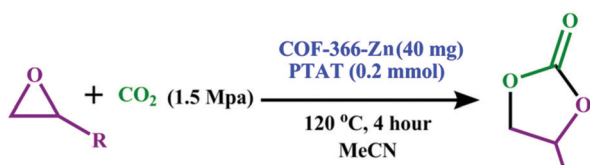
Fig. 8 (a) FTIR and (b) PXRD analysis of COF-366-M catalysts, and PXRD patterns of (c) COF-366-Co(2) and (d) COF-366-Co(1). Reproduced with permission from ref. 23; copyright: 2017, Dalton Transactions.

analog was used instead of BDA. COF-366 was combined with zinc acetate dihydrate and cobalt acetate dihydrate to prepare COF-366-Zn and COF-366-Co(1), respectively. The research group fabricated COF-366-Co(2) *via* linking BDA with $Co(OAc)_2 \cdot 2H_2O$. Based on Fourier-transform infrared spectroscopy (Fig. 8), the structure of the COF was confirmed. They gathered information about the crystallinity of the COF-366-Co(1) and COF-366-M species, as shown in Fig. 8. N_2 adsorption–desorption analysis of COF-366-Zn at 77 K reveals that zinc metal was incorporated into COF-366 with a 2 nm pore size.

H. Wang and co-workers used COF-366-Zn, COF-366-Co(1), COF-366-Co(2), COF-SQ-Zn, and COF-SQ-Co catalysts to synthesize cyclic carbonates *via* CO_2 fixation (Scheme 7) and found that the COF-366-Zn catalyst is more proficient (98.9% yield) than the others. They also observed that there was no effective impact when they used COF-366-Zn and phenyltrimethylammonium (PTAT) individually for cyclo-addition reactions involving CO_2. However, if COF-366-Zn is used with phenyltrimethylammonium, TPPB, tetrabutylammonium bromide, or dimethylaminopyridine as an auxiliary catalyst in methylcyanide solvent, the product yield becomes 98.9%, 99.2%, 71.2%, or 19.6%, respectively; the acceleration in the reaction rate could be attributed to the strong nucleophile Br^-, which works as an auxiliary metallic site during CO_2 cycloaddition reactions.[24]

Xiaoming Liu *et al.*, in 2018, studied metal-free COFs, namely COF-JLU6 and COF-JLU7, for their application in cycloaddition reactions of carbon dioxide with epoxides for the synthesis of cyclic carbonates.[25] 1,3,5-Tris-(4-aminophenyl)triazine (0.08 mmol) and 2,5-dihydroxy-benzene-1,4-dicarbaldehyde (0.12 mmol) were used as starting materials for the formation of COF-JLU6 under solvothermal conditions, and mesitylene/1,4-dioxane was used as the solvent. In a very similar way, COF-JLU7 was synthesized, but the solvent was different in this case: *o*-dichlorobenzene/*n*-butanol. One-dimensional oriented porous channels are present in both COF-JLU6 and COF-JLU7. The two synthesized COFs contain some heteroatoms and hydroxyl groups on their walls, which help to enrich the COFs with CO_2 and facilitate CO_2 fixation with epoxides (Fig. 9). The COFs possess a large BET surface area, approximately 1390 m^2 g^{-1}, with a suitable pore volume of 1.78 cm^3 g^{-1}. The carbon dioxide uptake capacity of COF-JLU7 is 151 g mg^{-1} at 273 K and 1 bar pressure. The characteristic C=O stretching frequency of the monomer at 1683 cm^{-1} also disappeared for both COFs. A strong stretching vibration was observed at 1584 cm^{-1} for COF-JLU6 and at 1582 cm^{-1} for COF-JLU7. They found a powder X-ray diffraction peak at a 2θ value of 2.82° for COF-JLU6 and some weak peaks at 2θ values of 4.82, 5.62, and 7.49 degrees, which correspond to the (100), (200), (210), and (220) reflection planes, respectively. Likewise, PXRD analysis of COF-JLU7 showed peaks at 2θ values of 2.67, 4.72, and 9.50 degrees.
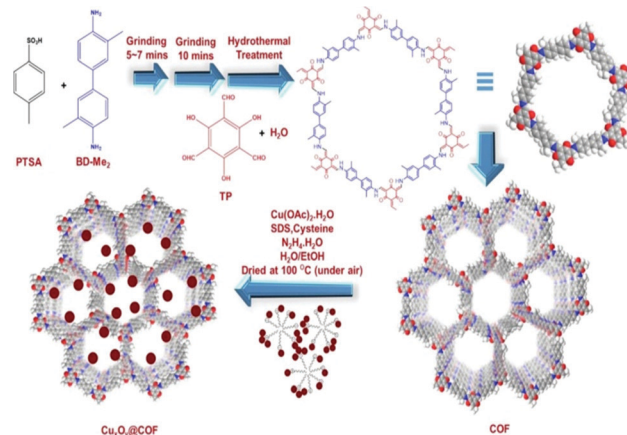
This research group confidently used COF-JLU6 and COF-JLU7 as elegant catalytic systems for the cycloaddition of carbon dioxide and epoxides to make cyclic carbonates under ambient conditions, as represented in Scheme 8. Here, they used tetrabutylammonium bromide as an auxiliary catalyst for the cycloaddition reactions and observed enhanced rates and yields during the reactions (approx. 86% in the case of COF-JLU6 and 92% for COF-JLU7). They concluded that COF-JLU7 showed a more satisfactory catalytic outcome compared to COF-JLU6. The group demonstrated a suitable mechanistic path
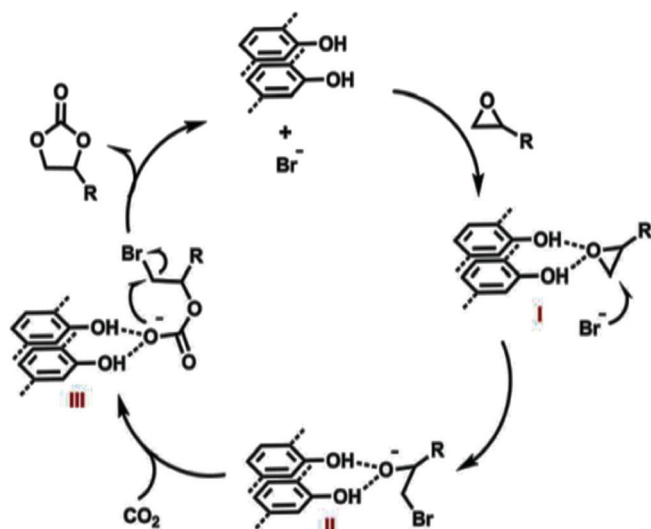

Scheme 7 The synthesis of cyclic carbonates *via* CO_2 incorporation using COF-366-Zn. Reproduced with permission from ref. 23; copyright: 2017, Dalton Transactions.

Fig. 9 (a) A diagram of the synthesis of COF-JLU6 and COF-JLU7 *via* condensation. (b) Top and (c) side views of [COF-JLU6]. (d) Top and (e) side views of [COF-JLU7]. Reproduced with permission from ref. 25; copyright: 2018, Journal of Materials Chemistry A.

Scheme 8 COFs (JLU6 and JLU7) used in cycloaddition reactions. Reproduced with permission from ref. 25; copyright: 2018, Journal of Materials Chemistry A.

Scheme 10 A schematic diagram of the synthesis of $Cu_xO_y@COF$. Reproduced with permission from ref. 26; copyright: 2019, Journal of CO_2 Utilization.

Scheme 9 A self-explanatory mechanistic path supporting the cycloaddition of CO_2 using COF-JLU7 and TBAB. Reproduced with permission from ref. 25; copyright: 2018, Journal of Materials Chemistry A.
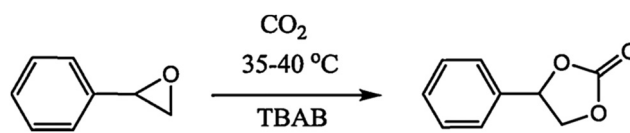
for the cycloaddition of CO_2 and epoxides using a COF-JLU7 and TBAB pair (Scheme 9).

In 2019, our research group headed by Prof. S. M. Islam reported that Cu_xO_y nanoparticles (Cu_2O and Cu_4O_3) could be used as an effective catalyst in cycloaddition reactions involving CO_2 when those nanoparticles were decorated on a covalent organic framework.[26] We synthesized the COF via a slight modification to the literature report by R. Banerjee et al.[27] To fabricate the COF, our group combined 2.5 mmol of para-toluenesulfonic acid with 0.45 mmol of 2-toluidine in a pestle and mortar and ground it for some time; then, 1,3,5-triformylphloroglucinol (0.3 mmol) was poured into the mixture. Lastly, the entire mixture was transferred into an autoclave and left at 100 °C overnight, and reddish-orange COF powder was obtained (Scheme 10). Later on, we added copper oxide (Cu_xO_y) nanomaterial to the surface of the covalent organic framework. It was observed that the low-angle X-ray

diffraction patterns of COF and $Cu_xO_y@COF$ show an acute peak at a 2θ value of $3.5°$ due to the (100) reflection plane, and it was observed that the COF remained unaltered even after decoration with copper oxide nanomaterial. The sharp peak at a 2θ value of $\sim 28.29°$ indicates the crystallinity of the substance, which remains unchanged even after Cu_xO_y incorporation.[28] The N_2 adsorption–desorption isotherm revealed that the synthesized copper-oxide-loaded COF exhibited a type-IV isotherm, which indicates the mesoporous nature of the $Cu_xO_y@$ COF material. It was observed that the total calculated surface coverage of COF, pristine $Cu_xO_y@COF$, and used $Cu_xO_y@COF$ were 460, 385, and 379 m^2 g^{-1}, respectively.

The $Cu_xO_y@COF$ material has been successfully applied in the cycloaddition of CO_2 to styrene oxide in the presence of the co-catalyst tetrabutylammonium bromide (5 mol%). A schematic representation of this reaction is given in Scheme 11. The research group carried out a time-on-stream (TOS) study, which revealed a gradual increase in the conversion of styrene oxide; after 12 h, the reaction yield became constant (approx. 92%). It was found that in the absence of $Cu_xO_y@COF$ and TBAB, the reaction did not proceed at all. A plausible reaction mechanism for the cycloaddition reaction was also demonstrated, as presented in Scheme 12.

In 2019, Jianji Wang and his research team reported a newly fashioned azine-linked 3D-COF named 3D-HNU5 which was applied fruitfully as a catalyst to support the cycloaddition reaction of propargyl alcohol with carbon dioxide to make cyclic carbonates.[29] Nowadays, 3D COFs receive huge attention due to their large surface areas and ample numbers of open sites.[30]

Scheme 11 The cycloaddition of CO_2 with styrene oxide using $Cu_xO_y@$ COF. Reproduced with permission from ref. 26; copyright: 2019, Journal of CO_2 Utilization.

Scheme 12 A probable mechanistic path for the synthesis of styrene carbonate *via* a cycloaddition reaction using the $Cu_xO_y@COF$ catalyst and TBAB as a co-catalyst. Reproduced with permission from ref. 26; copyright: 2019, Journal of CO_2 Utilization.

This research group synthesized an azine-linked 3D COF for the very first time. They synthesized the 3D-HNU5 COF *via* the condensation of tetrakis(4-formylphenyl)-methane in the ionic liquid [1-butyl-3-methylimidazolium bis(trifluoromethyl-sulfonyl)imide], as represented in Scheme 13. X-ray diffraction and simulation studies revealed that 3D-HNU5 COF has an interpenetrating diamond-like topology, with excellent crystallinity and high thermal stability. An SEM study revealed that the COF has rod-shaped morphology with dimensions of 0.5–1 micrometer. They performed PXRD analysis, and peaks were obtained at 2θ values of 7.75, 9.67, 10.97, 13.29, 14.89, 17.42, and 19.16 degrees corresponding to the (101), (111), (102), (003), (202), (221), and (311) reflection planes, respectively. The type-I isotherm obtained *via* N_2 adsorption–desorption studies at 77 K helped demonstrate the microporous properties

of the COF. The N_2-BET surface coverage was observed to be 864 m^2 g^{-1} for 3D-HNU5-COF. The research team obtained an impressive pore volume for this COF of 0.89 cm^3 g^{-1} at a P/P_0 value of 0.99.

Among different COFs, 3D COFs can be used for gas storage because of their great surface coverage, low densities, and many free sites.[31] The same research group used the three-dimensional HNU5 COF as a support for Ag metal and used this silver-embedded COF for CO_2 fixation using 2-methylbut-3-yn-2-ol under atmospheric pressure. It was found that the cyclo-addition reaction did not work in the absence of Ag nanoparticles, but with Ag@3D-HNU5 COF, the yield was up to 99% with a TON of 990 (Fig. 10).

Yu-Bin Dong *et al.*, in 2019, reported the synthesis of the ionic-liquid-immobilized COF presented in Scheme 14 and a newly fashioned COF-chitosan aerogel, and they studied the catalytic outcomes during the fixation of CO_2 with styrene oxide to form cyclic carbonates.[32] They prepared 1,3,5-triformyl-phloroglucinol according to a reported process.[33] Thiol-group-containing chitosan was prepared according to a reported method.[34] They also synthesized the three required precursors for IL-ADH according to previously reported processes with slight modifications.[35] The research group synthesized COF-IL@chitosan *via* blending COF-IL (1.35 g) and HMPP (150 μL) with an aqueous solution of acidic chitosan, as represented in Scheme 15. The group carried out ^{13}C-NMR CP-MAS studies to show the formation of COF-IL. The PXRD pattern of COF-IL@chitosan showed that its crystallinity and integrity were suitably maintained in the sponge-like aerogel.
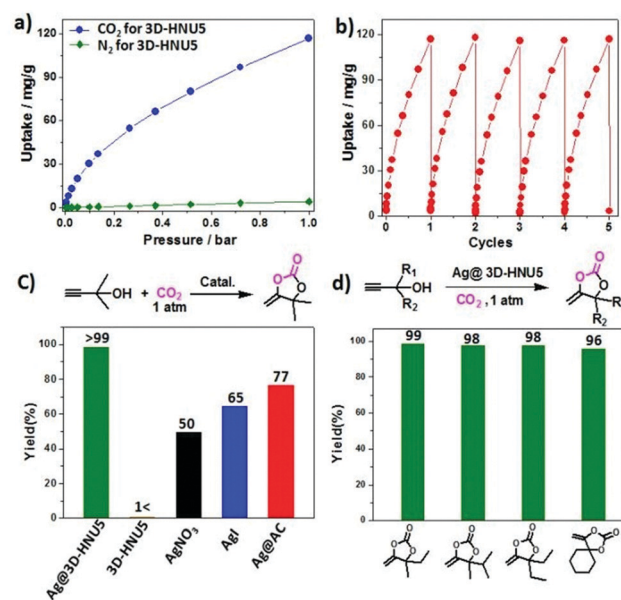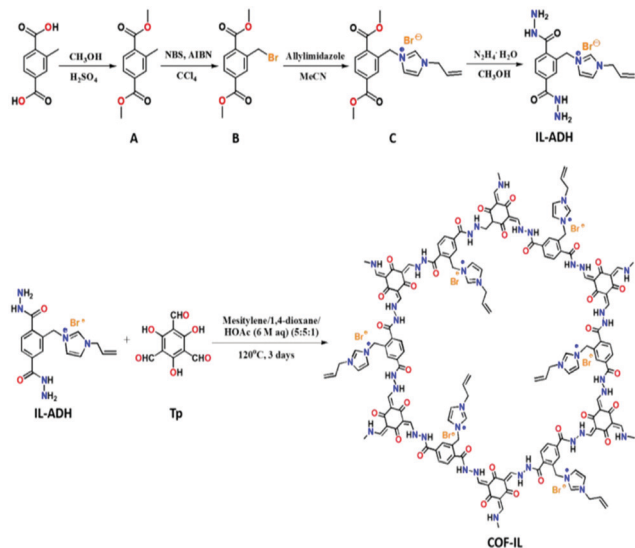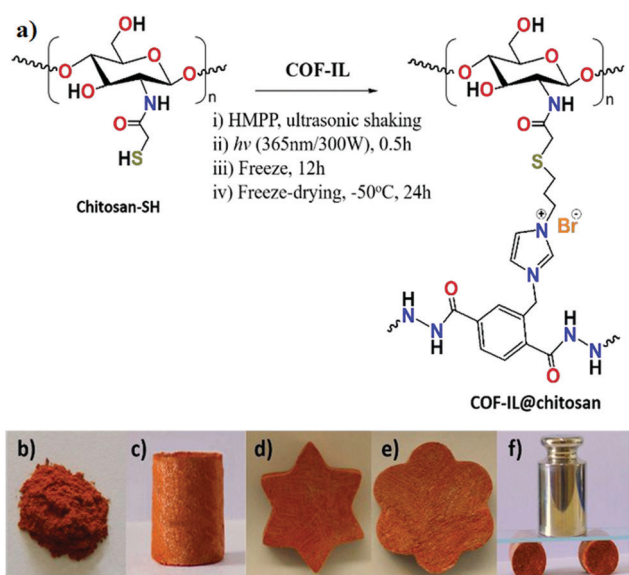

Scheme 13 (a) The synthesis of 3D-HNU5 COF and (b) its 3D perforated structure and 2-fold interpenetrating diamond-like frame (blue: C, white: H, red: N). Reproduced with permission from ref. 29; copyright: 2019, Chemical Communications.

Fig. 10 (a) CO_2 and N_2 isotherms for 3D-HNU5 COF at 273 K. (b) CO_2 adsorption by 3D-HNU5 over multiple cycles at 273 K. (c) A study of catalysts for the formation of cyclic carbonates. (d) The yield percentages of different cyclic carbonates when Ag@3D-HNU5 is used as the catalyst. Reproduced with permission from ref. 29; copyright: 2019, Chemical Communications.

Scheme 14 The synthesis of COF-IL and IL-ADH and their oriented structures. Reproduced with permission from ref. 32; copyright: 2019, Journal of Materials Chemistry A.

Scheme 15 (a) The synthesis of COF-IL@chitosan. Photographs of (b) COF-IL (solid-crystals) and (c–e) COF-IL@chitosan (aerogel) with different shapes. (f) The pressure testing of an aerogel column done with a weight of 250 g. Reproduced with permission from ref. 32; copyright: 2019, Journal of Materials Chemistry A.

They found COF-IL to be very efficient for use in CO_2 cycloaddition reactions (Fig. 11). COF-IL could be applied to many types of epoxides, except for long hexadecyl-connected epoxides. The researchers observed that under the optimized conditions, epichlorohydrin and epibromohydrin provided high yields of 98% and 100%, respectively, within 48 h. For actual applications, they prepared a cuplike reactor *in situ* and used the advantages of the COF@chitosan aerogel.

Another report was provided by Jianji Wang *et al.* in 2020. A standard acid–base reaction method was used to combine

Fig. 11 (a) The effects of temperature, reaction time, and catalyst amount on COF-IL-catalysed CO_2 cycloaddition to styrene oxide. (b) Reaction time analysis (black line) and leaching testing (red line) during CO_2 cycloaddition to styrene oxide catalyzed by COF-IL. (c) Recycling of the catalyst. (d) PXRD patterns from every catalytic cycle. Reproduced with permission from ref. 32; copyright: 2019, Journal of Materials Chemistry A.

an ionic liquid (imidazolium-salt-based) and covalent organic framework, and this material was applied as a catalyst to promote the formation of cyclic carbonates from carbon dioxide.[36] Firstly, they prepared an SO_3H-activated COF named TpPa–SO_3H, which has numerous Brønsted acid sites, and these sites could be utilized to immobilize the imidazolium salt, and eventually the COF was termed COF-HNU14 (Scheme 16). This COF-material showed very high crystallinity during nanoscale measurements of the pores. COF-HNU14 performed excellently in CO_2 cycloaddition with epoxides. Condensation between 1,3,5-triformylphloroglucinol and 2,5-diaminobenzenesulphonic acid resulted in the formation of the TpPa–SO_3H material. The group prepared red crystals with an isolated TpPa–SO_3H yield of $\sim$82% *via* mixing Tp (0.5 mmol) and Pa–SO_3H (183 mg, 0.75 mmol)
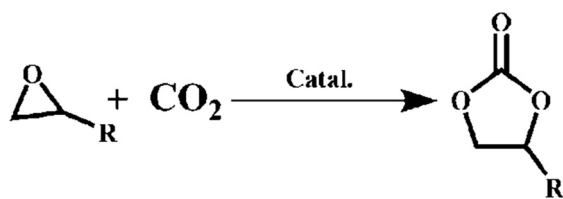

Scheme 16 The synthesis of TpPa–SO_3H and COF-HNU14. Reproduced with permission from ref. 36; copyright: 2020, ACS Sustainable Chemistry & Engineering.

under the catalytic acceleration of acetic acid at 120 °C for three days. They studied the PXRD patterns to clarify the structure of the TpPa–SO$_3$H material. TpPa–SO$_3$H showed peaks at 2θ values of 4.4, 8.1, and 25 degrees corresponding to the (100), (110), and (001) planes, respectively. The (001) reflection confirms the π–π stacking of the planes and the pattern resembled an AA stacking model.[37] N$_2$ adsorption–desorption isotherm studies revealed the permanent porous nature of TpPa–SO$_3$H at 77 K. The research group calculated the surface area with the help of BET analysis and found that the coverage is 294 m^2 g^{-1}, and the pore volume of TpPa–SO$_3$H is 0.41 cm^3 g^{-1}. They fabricated COF-HNU14 *via* mixing TpPa–SO$_3$H with an aqueous solution of 1-aminopropyl-3-methylimidazolium bromide at room temperature. BET analysis revealed that COF-HNU14 has a lower surface area of 196 m^2 g^{-1} compared to TpPa–SO$_3$H.

Wang *et al.* found that cycloaddition reactions between carbon dioxide and epoxides were highly atom-economical when COF-HNU14 was used as the catalyst material, as shown in Scheme 17. It was observed that the cyclic carbonate yield was up to 99% when COF-HNU14 was used as the catalyst in the absence of any co-catalyst. This enhanced catalytic performance of the COF is ascribed to the nano-range order of the catalyst.[38] Cycloaddition between CO$_2$ and various epoxide substrates was performed, and it was observed that in the case of 2-chloromethyl oxirane and 2-bromomethyl oxirane substrates, the yields were maximal ($\sim$99%).

This research group proposed a three-step mechanistic route, based on the Gibbs free energy (Fig. 12), for cyclic carbonate synthesis, collecting information from some previous

Fig. 13 Optimized geometries for the transition states highlighted in Fig. 12. Reproduced with permission from ref. 36; copyright: 2020, ACS Sustainable Chemistry & Engineering.

reports. They also proposed optimized geometries for the transition states TS1, TS2, and TS3 (Fig. 13).

Long Chen *et al.*, in 2020, reported different covalent organic frameworks with structural similarities that could be used as metal-free immiscible catalysts for CO$_2$ cycloaddition.[39] Four different types of blocks were used for the TPBP ring-core, including 2,2′-dihydroxyl-3,3′,5,5′-tetrakis(4-formylphenyl)biphenyl (OH-TFBP), OMe-TFBP, 2,2′,-dimethoxy-3,3′,5,5′-tetrakis-(4-aminophenyl)biphenyl (OMe-TABP), and OH-TABP, and they were used as frames to build three separate COFs having different docking regions in a solvothermal environment and *via* a Schiff base poly-condensation method (Scheme 18). Solid-state ^{13}C-NMR spectra were obtained to establish the formation of the imine linkages. PXRD measurements gave diffraction peaks at 2θ values of 5.52, 8.05, and 11.05 degrees which were indexed to the (110), (200), and (220) planes, respectively, for the OMe-OH-TPBP material (Fig. 14).

This research group studied the cycloaddition reactions between CO$_2$ and various ethylene oxides. The methoxy COF analogue (OMe-OH-TPBP) showed the best catalytic performance during CO$_2$ fixation reactions to produce cyclic carbonates. Under the optimized conditions, OMe-OH-TPBP (COF) showed a 96% yield for CO$_2$ cycloaddition with epibromohydrin. The reaction yield was about 90% for the commercially

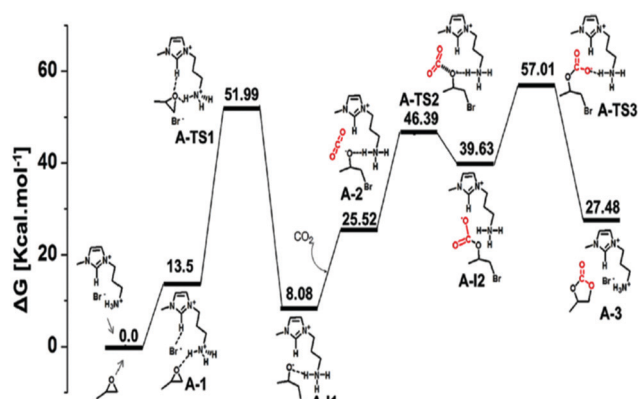**Scheme 17** The cycloaddition of CO$_2$ with substituted epoxides.

Fig. 12 COF–HNU14-catalyzed free-energy profiles for cyclic carbonate synthesis. Reproduced with permission from ref. 36; copyright: 2020, ACS Sustainable Chemistry & Engineering.
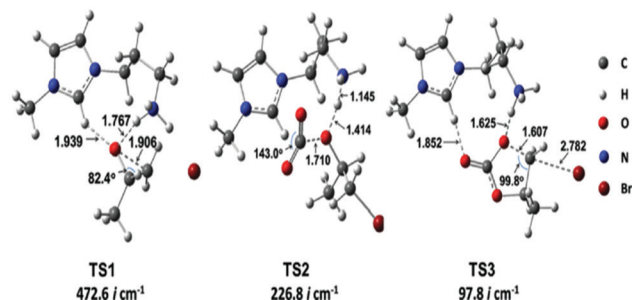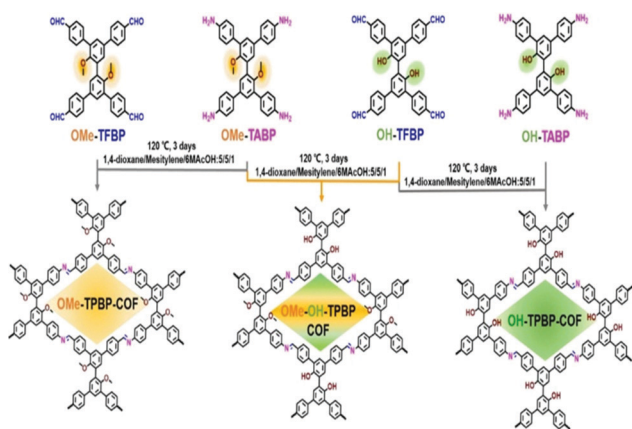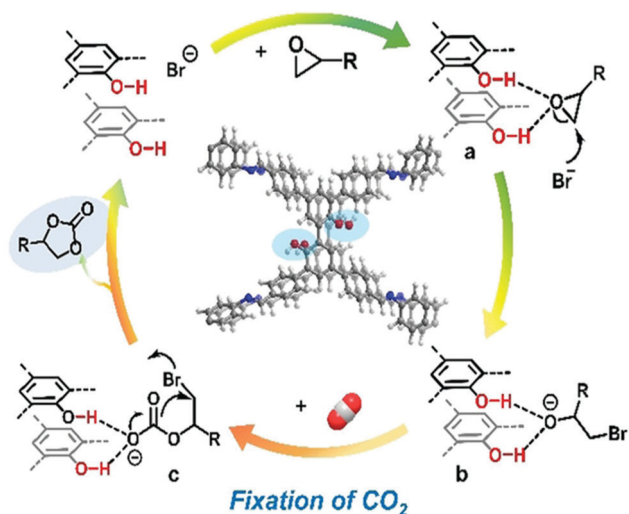
Scheme 18 The synthesis of OMe-TPBP, OMe-OH-TPBP, and OH-TPBP COF. Reproduced with permission from ref. 39; copyright: 2020, Chemistry A European Journal.
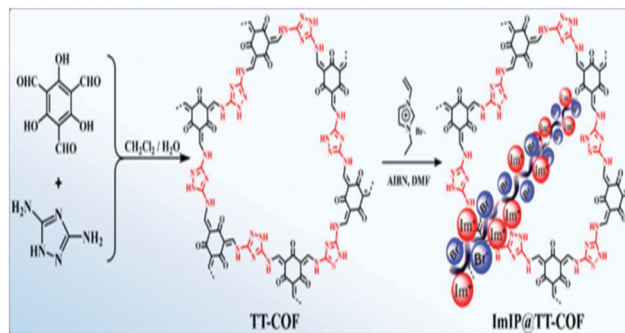
Fig. 14 (a) The powder XRD patterns of OMe-OH-TPBP-COF: experimentally observed (red), Pawley refinement (blue), and the difference (green), and simulations of AA-stacking (light blue) and AB-stacking (pink), (b) top and side views of OMe-OH-TPBP-COF. Reproduced with permission from ref. 39; copyright: 2020, Chemistry A European Journal.

Scheme 20 The synthesis of ImIP@TT-COF. Reproduced with permission from ref. 40; copyright: 2020, ChemSusChem.

by polymerization in azobisisobutyronitrile to generate ImIP@TT-COF (Scheme 20). They ascertained the structure and composition *via* performing FT-IR spectroscopy, solid-state ^{13}C-NMR, and powder X-ray diffraction studies. They observed the disappearance of the carbonyl peak of triformylphloroglucinol at 1647 cm^{-1} in the FT-IR spectrum of TT-COF, while C=C and C–N stretching signals were observed at 1593 and 1261 cm^{-1}, respectively. From ^{13}C-NMR analysis, they observed peaks at 136, 122, 45, 37, 31, and 14 ppm in the ImIP@TT-COF spectrum, illustrating the unification of ImIP (ionic polymer) with TT-COF. The powder XRD pattern of TT-COF revealed a pattern similar to previously reported results.[43]

The kinetic curves obtained for ImIP@TT-COF during the catalytic reaction are demonstrated in Fig. 15. The authors observed simultaneous increases in the formation of 4-chloro-methyl-[1,3]dioxolan-2-one and the consumption of 2-chloromethyl-oxirane, with completion within 8 h. They studied the temperature-
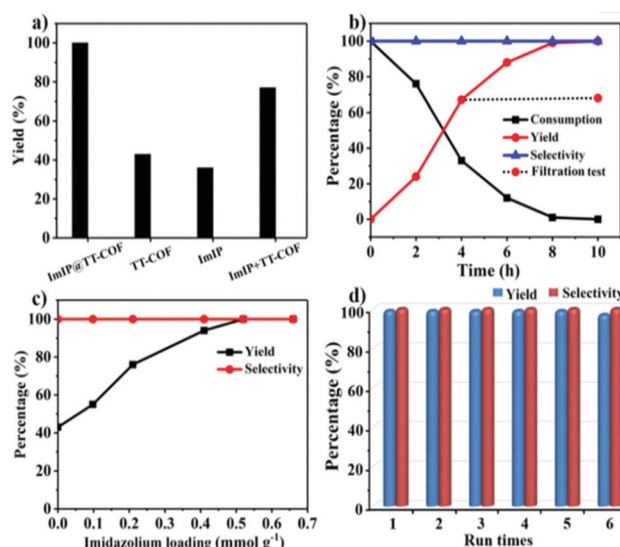

Scheme 19 A probable mechanism for CO_2 cycloaddition with ethylene oxides using methoxy-hydroxyl-TPBP-COF and tetrabutylammonium bromide. Reproduced with permission from ref. 39; copyright: 2020, Chemistry A European Journal.

vital epoxypropane, and the yield was slightly lowered in the case of epoxides with long alkyl-chain lengths. They also studied a possible reaction mechanism for CO_2 fixation with epoxides where the catalyst OMe-OH-TPBP-COF and tetrabutyl-ammonium bromide were used, as presented in Scheme 19.

After that, in 2020, Ruihu Wang *et al.* reported an acceptor–receptor catalytic analog *via* combining an imidazolium-based ionic polymer and a nitrogen-filled covalent organic framework (TT-COF), and this supported CO_2 cycloaddition.[40] Among the available catalytic methodologies for CO_2 cycloaddition with epoxides, this is an atom-economical and environmentally benign method.[41] They showed that immobilizing the ionic liquid (imidazolium analog) on the wall of the COF improves the catalytic abilities in the absence of co-catalysts and other materials.[42] The group prepared TT-COF *via* mixing 1*H*-[1,2,4]-triazole-3,5-diamine and *para*-toluenesulfonic acid in a dichloro-methane solution of 2,4,6-triformylphloroglucinol (TP). Then, they performed an ultrasonic reaction of TT-COF with 3-ethyl-1-vinyl-imidazolium salt dissolved in *N,N*-dimethylformamide, followed

Fig. 15 (a) The catalytic activities of ImIP@TT-COF, ImIP, TT-COF, and a blend of imidazolium salt and TT-COF. (b) Kinetic curves for the CO_2 cycloaddition reaction. (c) The impact of ImIP content. (d) The recyclability of the COF. Reproduced with permission from ref. 40; copyright: 2020, ChemSusChem.

dependency under atmospheric CO_2 over a temperature range of 25 to 140 °C. It was observed that comparatively higher temperatures have a good effect on CO_2 fixation. At 120 °C, conversion was the most effective. The impact of 3-alkyl-1-vinyl-imidazolium attachment to TT-COF on catalytic conversion was also studied. The percentage yield of 4-chloromethyl-1,3-dioxolan-2-one was increased when the ImIP content reached 7.2 wt%, and the approximately linear relationship between catalytic activity and electron-rich Br^- species content was revealed.

Wei-Qiao Deng *et al.*, in 2020, reported a COF named Zn-salen-COF-SDU113 which was developed through a 'pore enrichment' technique and applied to CO_2 cycloaddition to epoxides.[44] They previously showed that a salen-conjugated perforated polymer can accelerate CO_2 fixation and can convert CO_2 to value-added chemicals.[45] In this article, they used a large-scale computational screening technique to determine the best candidate from a COF library and present the suitably predicted COF. Firstly, the authors built a virtual library of 10 994 COFs utilizing salen-metal as the active center. Then, they synthesized the best COF, named Zn-salen-COF-SDU113 (COF), and studied its activity as a catalyst for CO_2 fixation. CO_2 cycloaddition can also be done with terminal epoxides and internal epoxides (*e.g.*, 2,3-epoxybutane) using Zn-salen-COF-SDU113 (COF) as the catalyst. This research group constructed a library of salen-COFs *via* choosing three kinds of linker groups to vary the structure of the COF. Thus, 27 metal elements were used as catalytic centers and different alkane substituents present in the salen molecule were taken into consideration during the formation of the salen-COFs (Fig. 16). The structures that were constructed helped with CO_2 enrichment. For Zn-salen-COF-SDU113, the amount of CO_2 adsorption is 3.99 mol g^{-1} (maximum value), and the second highest value of 3.94 mol g^{-1} is obtained with the Fe-salen compound.

In the case of CO_2 cycloaddition reactions with a terminal epoxide, Zn-salen-COF-SDU11 afforded a yield of 84.2% and a TON of 1142.7, while Zn-salen-COF-SDU113 had a yield of 98.2% and a TON of 3068.9 (Fig. 17).

In 2020, Yanan Gao *et al.* reported a two-dimensional COF attached to a 3-methyl-1-alkyl-3*H*-imidazol-1-ium salt, which was named AMIMBr@H_2P-DHPh-COF and used for cycloaddition reactions between epoxides and CO_2.[46] Among different available catalysts, various ionic liquids (ILs), *e.g.*, those based on ammonium salts,[47] phosphonium,[48] imidazolium,[49] and pyridinium cations,[50] have already shown extraordinary catalytic performance during carbon dioxide fixation reactions. The authors performed the immobilization of the ionic liquid on the channel barriers of a H_2P-DHPh COF *via* a specific method (Scheme 21).

The PXRD analysis and simulations illustrated the crystalline nature of the COF. X-ray diffraction peaks for H_2P-DHPh COF were observed at 2θ values of 3.5, 7.1, and 22.9 degrees that were attributed to the (100), (200), and (001) reflection planes. The authors also investigated a similar COF named BuBr@H_2P-DHPh COF.

This research group showed that the AMIMBr@H_2P-DHPh COF is very efficient during the cycloaddition of CO_2 and

Fig. 16 The synthesis of salen-COF. Reproduced with permission from ref. 44; copyright: 2020, Nature Communications.
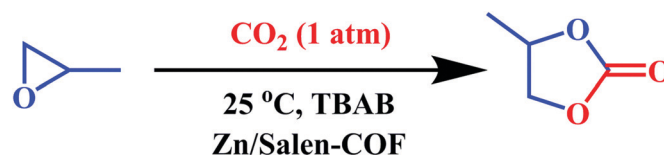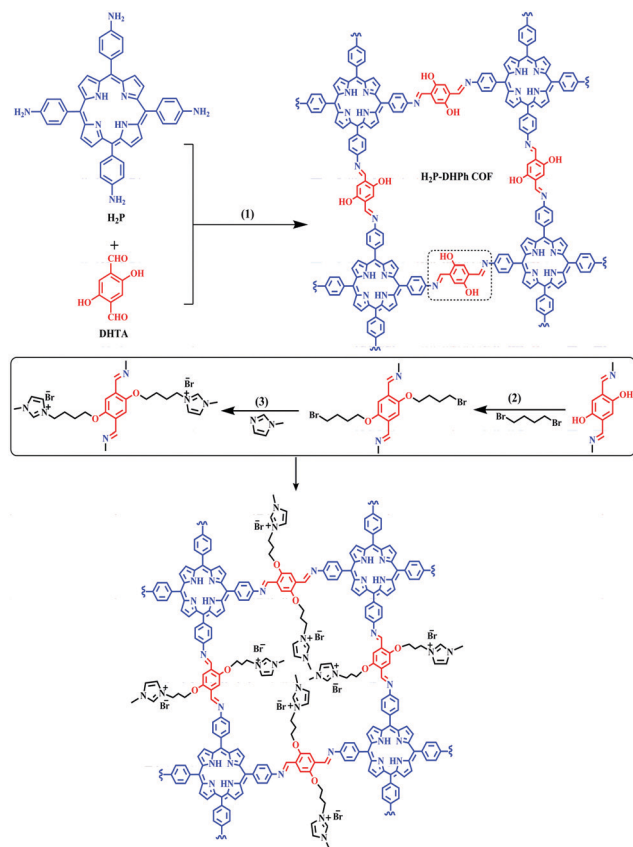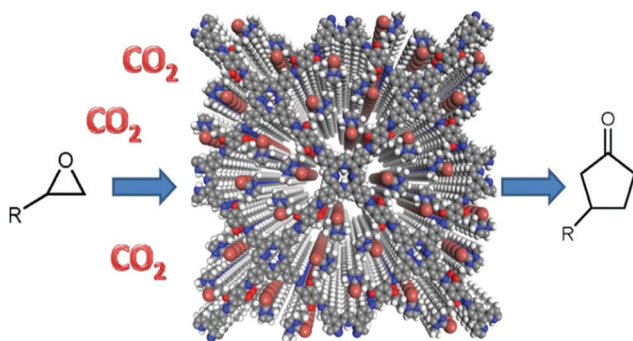

Fig. 17 Cycloaddition involving CO_2 and a terminal epoxide catalyzed by Zn-salen-COF-SDU113.

epoxides, and the yield is 91% for the substrate epichlorohydrin. However, using the catalyst H_2P-DHPh COF, the yield with the same substrate (epichlorohydrin) is only 40%, while without any additives the cycloaddition yield between epichlorohydrin and CO_2 is 38%. The authors have also studied different substrate variations (epoxide derivatives) and the catalytic performance of the AMIMBr@H_2P-DHPh COF during these reactions (Scheme 22).
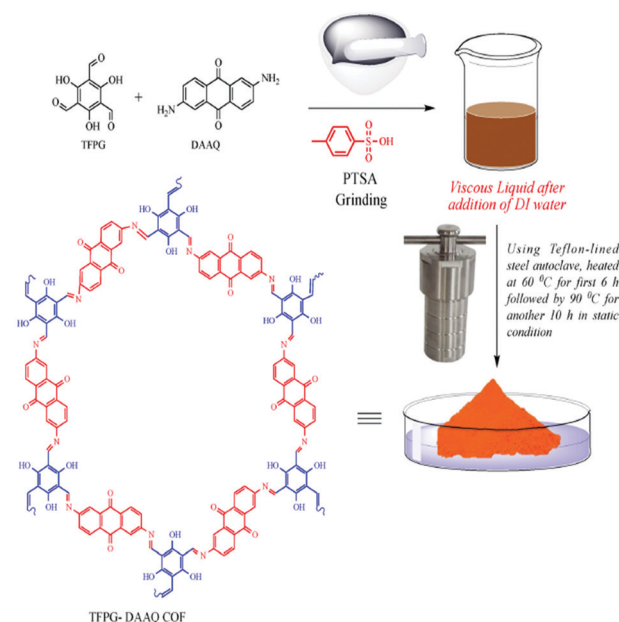
In 2019, our research group synthesized a porous TFPG-DAAQ COF photocatalyst (Scheme 23) for the synthesis of formic acid from atmospheric CO_2.[51] Our group developed the COF *via* heating 1,3,5-triformylphloroglucinol and 2,6-diaminoanthraquinone (DAAQ) with *p*-toluenesulfonic acid (PTSA) in a steel autoclave with an inner Teflon lining at 60 °C for 6 h and for another 10 h at 90 °C under nondynamic conditions.

Scheme 21 The synthesis of AMIMBr@H$_2$P-DHPh COF.

Scheme 22 Cycloaddition reactions using AMIMBr@H$_2$P-DHPh COF. Reproduced with permission from ref. 46; copyright: 2020, Chinese Journal of Catalysis.

Scheme 23 The synthesis of TFPG-DAAQ COF. Reproduced with permission from ref. 51; copyright: 2020, Molecular Catalysis.

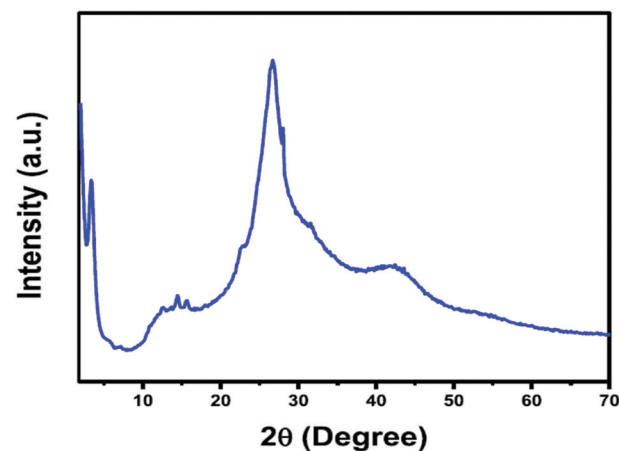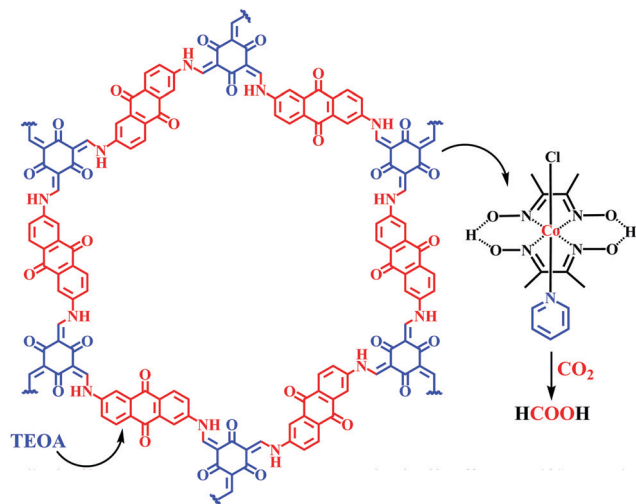Fig. 18 PXRD analysis of TFPG-DAAQ. Reproduced with permission from ref. 51; copyright: 2020, Molecular Catalysis.

Our team has performed numerous characterization studies to ascertain the structure of TFPG-DAAQ COF (Fig. 18). There are two characteristic peaks present in the PXRD pattern of TFPG-DAAQ COF at 2θ values of 27.1° and 3.5°, confirming the presence of (001) and (100) diffraction planes, respectively. The peak at a 2θ value of 27.1° arises due to the π–π synergy of the (001) plane. From the FT-IR spectra of DAAQ, TFPG, and the TFPG-DAAQ COF catalyst, we can confirm the successful complexation reaction between DAAQ and TFPG.

The TGA results for the TFPG-DAAQ COF show that the COF is thermally stable up to 425 °C. With the help of N$_2$ sorption studies involving the TFPG-DAAQ COF catalyst, we showed that the TFPG-DAAQ COF has a pore diameter of 3.8 nm; the pores are narrow and have a uniform pore-size distribution. This classifies the catalyst as mesoporous, and the calculated BET surface area of the TFPG-DAAQ COF is observed to be 600 m^2 g^{-1}, with a total pore volume of 0.81 cm^3 g^{-1}.

Our group demonstrated the conversion of triethanolamine with the assistance of the TFPG-DAAQ COF catalyst under a CO$_2$ atmosphere and irradiation at 445 nm and 12 W cm^{-2} at room temperature, and we obtained an excellent yield of formic acid with a turnover number of 125. We also used Co(dmg)$_2$ as a co-catalyst for this reaction. We proposed that the same reaction can be executed even in the presence of ambient sunlight at a slower rate, having a TON of 36. From this study, we
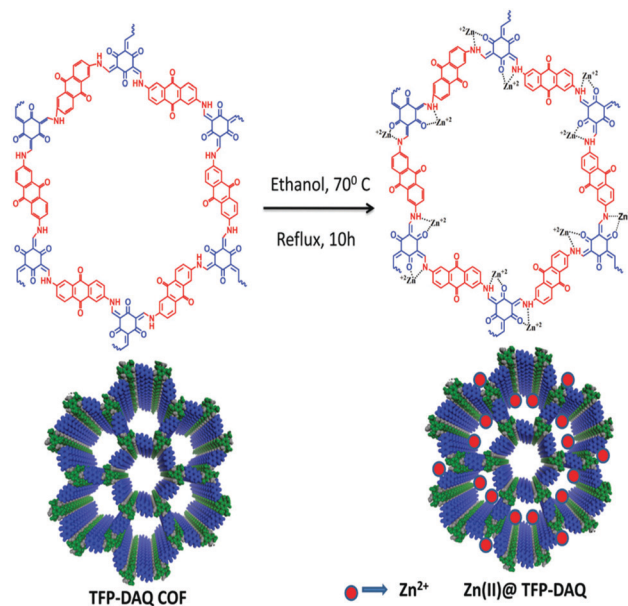
Scheme 24 The synthesis of HCOOH.

concluded that the completely heterogeneous TFPG-DAAQ COF catalyst can be recycled up to five times without any prominent change in its catalytic activity. It was observed that the TON of the isolated product decreases from 125 to 0 in the absence of the TFPG-DAAQ COF catalyst. Based on all these experimental observations, this TFPG-DAAQ COF catalyst was identified as an excellent one for formic acid preparation (Scheme 24).

2.3 Carbamate syntheses

Our team, in 2019, reported a zinc-loaded COF material designated as Zn(II)@TFP-DAQ COF.[52] We synthesized this COF base catalyst through the loading of anhydrous $ZnCl_2$ on a TFP-DAQ COF in methanol solvent. Our team performed several characterization studies to establish the structure of this zinc-loaded COF (Scheme 25). The PXRD pattern of the zinc-loaded COF showed two characteristic peaks at 2θ values of $3.6°$ and $27.2°$, which indicate the presence of the (100) and (001) planes, respectively, as represented in Fig. 19. Of these two intense peaks, the second arises due to $\pi-\pi$ interactions involving the (001) plane.[53] Our research group also performed XPS analysis, which showed that the oxidation state of zinc in the Zn(II)@TFP-DAQ COF is 2+. The total calculated BET surface area of the synthesized mesoporous Zn(II)@TFP-DAQ COF catalyst is $1117.375 \ m^2 \ g^{-1}$ with a pore volume of $1.31 \ cm^3 \ g^{-1}$. This admirable surface area allows this synthesized Zn(II)@TFP-DAQ COF catalyst to show tremendous performance during carbamate synthesis *via* CO_2 fixation.

Our research group has synthesized both alkyl and aryl carbamates at room temperature under atmospheric pressure, starting from different aniline substrates, *via* CO_2 fixation reactions using the Zn(II)@TFP-DAQ catalyst in DMSO solvent at room temperature and in the absence of base (Scheme 26). We reported that this reaction is completed within 8 h with an extraordinary carbamate yield of 97%. Aniline and alkyl bromide were used as starting materials during carbamate synthesis under CO_2 at atmospheric pressure. We demonstrated that this completely heterogeneous catalyst can be

Scheme 25 The synthesis of a zinc-loaded porous@TFP-DAQ COF. Reproduced with permission from ref. 52; copyright: 2020, New Journal of Chemistry.
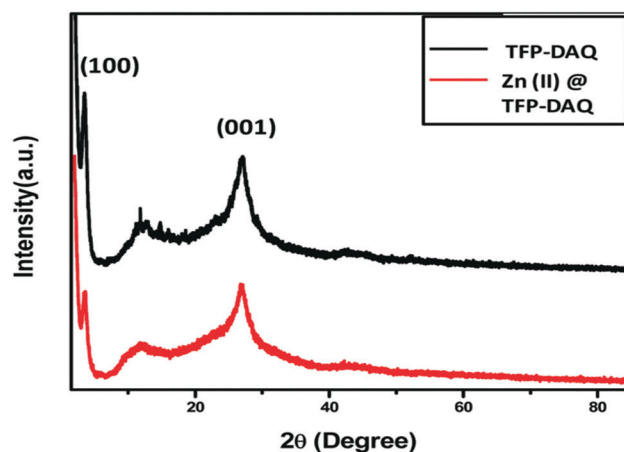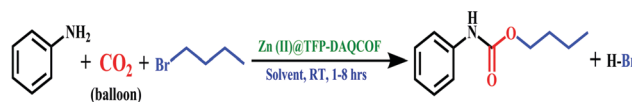

Fig. 19 The PXRD analysis of TFP-DAQ COF and Zn(II)@TFP-DAQ COF. Reproduced with permission from ref. 52; copyright: 2020, New Journal of Chemistry.

Scheme 26 Butyl *N*-phenyl carbamate synthesis *via* carbon dioxide fixation.

recycled five times with almost no change in catalyst activity. We also carried out the same reaction in the absence of the catalyst and observed that there is a huge difference in yields of the catalytic and non-catalytic pathways, showing this catalyst to be superior during carbamate synthesis.

After that, in 2020, our research group reported a silver-loaded COF, designated as Ag/TFPG-DMB, for carbamate

Scheme 27 The synthesis of Ag/TFPG-DMB COF. Reproduced with permission from ref. 54; copyright: 2020, Molecular Catalysis.
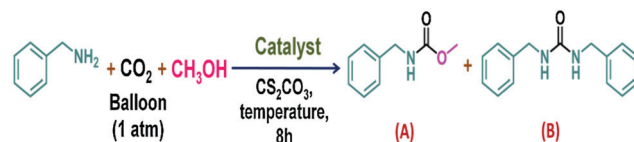

Scheme 28 Methyl benzyl carbamate synthesis *via* a CO_2 fixation reaction. Reproduced with permission from ref. 54; copyright: 2020, Molecular Catalysis.

synthesis *via* CO_2 fixation reactions.[54] We prepared the TFPG-DMB COF from 1,3,5-triformylphloroglucinol (TFPG) and DMB using *p*-toluenesulfonic acid (PTSA) through hydrothermal treatment, and we then decorated the TFPG-DMB COF with silver nanoparticles *via* a previously reported method (Scheme 27).[55]

Our group has performed numerous characterization studies to determine the structure of the silver-loaded COF. The PXRD pattern (Fig. 20) of this silver-loaded COF showed a characteristic peak at a 2θ value of $3.5°$ due to the (100) plane and a peak at $26.39°$ which implies the presence of the (001) plane due to the π–π interactions of (001) planes. Four characteristic peaks from metallic Ag were also observed at 2θ values of $44.56°$, $64.31°$, $38.17°$, and $77.31°$, indicating the presence of the (220), (200), (111), and (311) crystal planes, respectively. With the help of N_2 adsorption–desorption isotherms, we identified that this COF catalyst is a mesoporous one, having a pore diameter of 3.9 nm, and the calculated BET surface area and total pore volume of this COF are found to be $651.64\ m^2\ g^{-1}$ and $0.36\ cm^3\ g^{-1}$. This high surface area makes this catalyst an excellent one for carbamate synthesis.

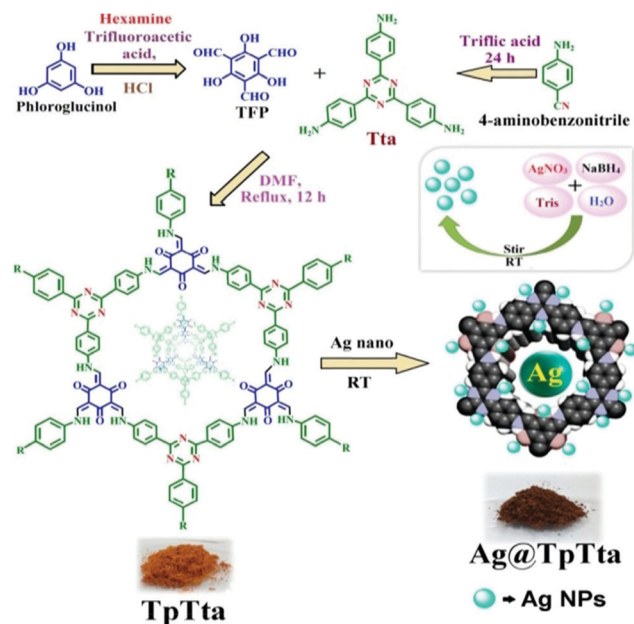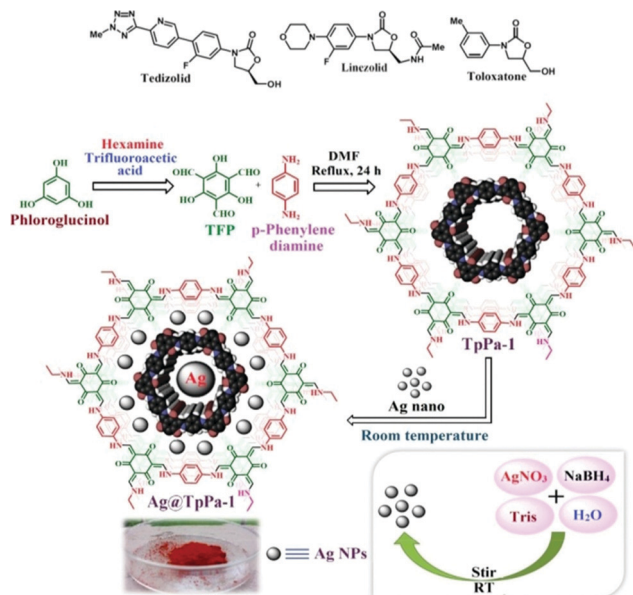Our team treated various benzylamine derivatives in the presence of the Ag/TFPG-DMB COF as a catalyst, using Cs_2CO_3

as a base and methanol as a solvent under CO_2 at atmospheric pressure at 80 °C for 8 h, and we obtained an excellent carbamate yield of 97%, as represented in Scheme 28. We proposed that this completely heterogeneous catalyst can be recycled five times with minimal changes in the activity of the catalyst. When we carried out the reaction in the absence of catalyst, it was observed that the yield of isolated product diminished to 2% from 97%, showing the catalyst to be superior for carbamate synthesis.

After this successful work, we demonstrated another interesting work[56] in which the silver-loaded COFs Ag@TpPa-1 and Ag@TpTta were fabricated and applied in carbamate synthesis. At first, we synthesized TpPa-1 *via* mixing exact quantities of triformylphloroglucinol and *p*-phenylene diamine in the presence of DMF solvent. TpTta, a covalent framework, was synthesized from (1,3,5-triazine-2,4,6-triyl)-trianiline (Tta), triformylphloroglucinol, and 4-aminobenzonitrile. A special characteristic of the synthesized COFs is that the materials are highly enriched with N atoms, which can hold Ag nanoparticles effectively, and the materials are also alkali free (Schemes 29 and 30).[56] The PXRD patterns of both the catalysts revealed highly intense and exceptional peaks at 2θ values of ~4.8 degrees for Ag@TpPa-1 and ~5.8 degrees for the COF in the

Fig. 20 PXRD analysis of Ag/TFPG-DMB COF. Reproduced with permission from ref. 54; copyright: 2020, Molecular Catalysis.

Scheme 29 The synthesis of Ag@TpTta. Reproduced with permission from ref. 56; copyright: 2020, ACS Sustainable Chemistry & Engineering.

Scheme 30 The synthesis of Ag@TpPa-1. Reproduced with permission from ref. 56; copyright: 2020, ACS Sustainable Chemistry & Engineering.
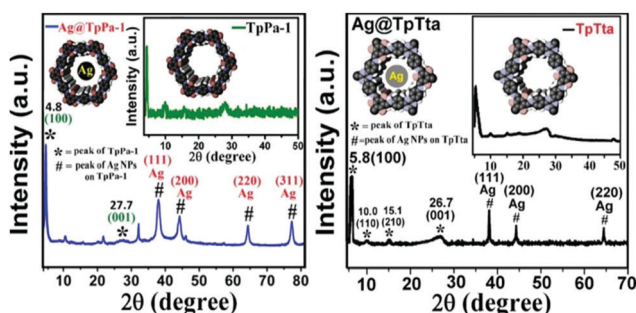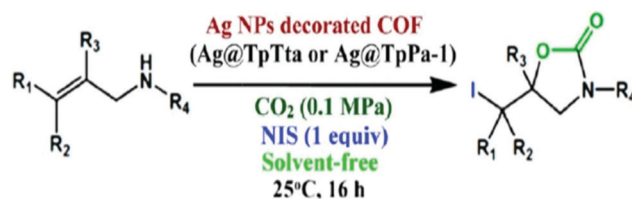

Fig. 21 The powder XRD patterns of Ag@TpPa-1 and Ag@TpTta. Reproduced with permission from ref. 56; copyright: 2020, ACS Sustainable Chemistry & Engineering.

nanocatalyst (Ag@TpTta), corresponding to the (100) plane, as represented in Fig. 21.[57] The two extra peaks at 2θ values of ~15.1 and 10.0 degrees correspond to the (210) and (110) planes, respectively. According to the PXRD pattern, the peak at a 2θ value of 27.7° (for Ag@TpPa-1), attributed to the (001) plane, was observed due to π–π stacking between the benzene rings of two adjacent layers of the TpPa-1 cage. N_2 adsorption measurements confirmed that the 'Ag@TpPa-1' COF has a hugely perforated orientation with a surface area of 243 m^2 g^{-1}.

The previously mentioned Ag@TpTta COF reported by our group was also used to perform various carbamate formation reactions with allylamine and NIS at room temperature using DMSO as a solvent, as represented in Scheme 31; we observed an excellent cyclic carbamate yield of 96%, whereas we got a satisfactory cyclic carbamate yield of 86% under the same conditions when using the Ag@TpPa-1 COF. However, under solvent-free conditions, our group obtained a carbamate yield of 89% using the Ag@TpPa-1 COF. From experimental observations,
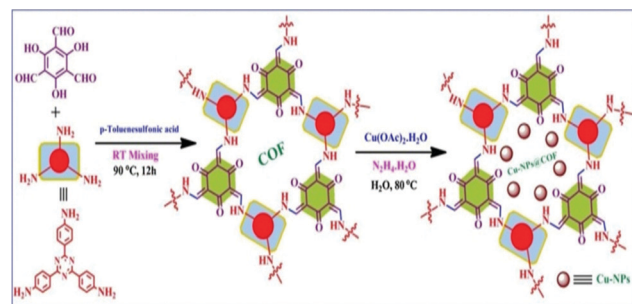

Scheme 31 The synthesis of carbamate using Ag@TpTta/Ag@TpPa-1 COFs. Reproduced with permission from ref. 56; copyright: 2020, ACS Sustainable Chemistry & Engineering.

we have concluded that Ag@TpTta performed better than Ag@TpPa-1, and the Ag@TpTta COF was selected for this CO_2-capture reaction. We showed in our research paper that there is a huge difference in the isolated product yields of the catalytic and noncatalytic pathways, making the catalyst superior for carbamate synthesis.

2.4 Oxazolidinone synthesis

Our research group also reported a copper-nanoparticle-loaded COF material, designated as Cu-NPs@COF, as represented in Scheme 32.[58] In our study, we synthesized the COF support using 2,4,6-triformylphloroglucinol and 4,4′,4″-(1,3,5-triazine-2,4,6-triyl)trianiline and performed different characterization studies to establish the structure of the copper-nanoparticle-loaded COF. From the XRD study, a broad peak was observed at a 2θ value of 26.71° due to π–π stacking involving the (001) reflection plane of the COF.[59] Then, we also found that the particle size of the designed material is around 0.5 nm.[60] It was clearly established from an XPS study that the oxidation state of copper is zero due to successful nanoparticle formation.

The members of our team synthesized 2-oxazolidinones under atmospheric pressure, starting from different propargyl amine substrates, *via* CO_2 fixation reactions at 50 °C using Cu-NPs@COF in MeCN solvent (Scheme 33). We reported that the reactions were completed after 12 h with excellent 2-oxazolidinone yields (95%). Our group found that using DBU as a base during 2-oxazolidinone synthesis provided maximum yields compared to other commercially available bases like Et_3N, Cs_2CO_3, K_2CO_3, and DABCO. It was also established that an increase or decrease in the reaction temperature from the optimum level decreased the yield of the product. Our team specified in the study that the designed

Scheme 32 The synthesis of Cu-NPs@COF. Reproduced with permission from ref. 58; copyright: 2020, Journal of CO_2 Utilization.
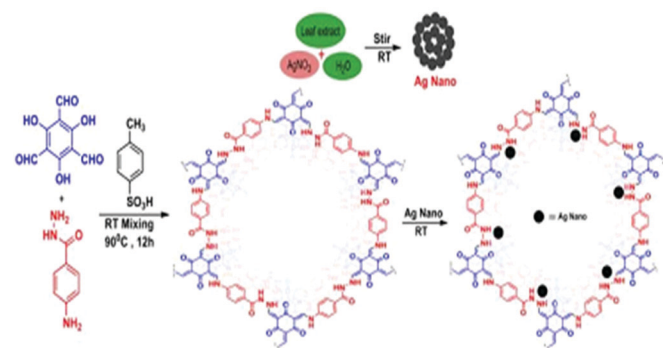
Scheme 33 A general synthesis scheme for 2-oxazolidinones. Reproduced with permission from ref. 58; copyright: 2020, Journal of CO_2 Utilization.

catalyst is recyclable for up to six cycles with only small changes in the product yields; this makes the catalyst excellent for 2-oxazolidinone synthesis.

In 2020, our research group reported another interesting work;[61] we developed a silver-nanoparticle-loaded COF material, termed AgN@COF, as a competent catalytic system for CO_2 fixation reactions. We designed the COF using 2,4,6-triformylphloroglucinol and 4-aminobenzoic acid hydrazide in the presence of *p*-toluenesulphonic acid. The Ag nanoparticles were synthesized (Scheme 34) *via* a green technique using leaf extract from *Cantana Camara*. We have used several characterization techniques to establish the structure of the COF embedded with silver nanoparticles. The PXRD spectrum of the COF revealed a peak at a 2θ value of $5.6°$ that corresponds to the (100) reflection plane and, in addition, a π–π stacking plane (001) signal was noticed over a wide 2θ range around $27.9°$.[62] We have performed high-resolution XPS analysis and showed that the 3d sub-shell of Ag suitably resembled the Ag 3d shell of Ag(0), which indicates that Ag(0) is embedded in the COF surface.[63] From N_2-BET adsorption–desorption isotherms, our team found that the total surface-areas of the synthesized COF and AgNPs@COF are 167 m^2 g^{-1} and 247.53 m^2 g^{-1}, respectively. Also, from TGA analysis, it was demonstrated that the designed catalyst is stable up to 250 °C. We observed micropores with a size of *ca.* 1.6 nm in the overall sample based on HRTEM images of AgNPs@COF (Fig. 22).
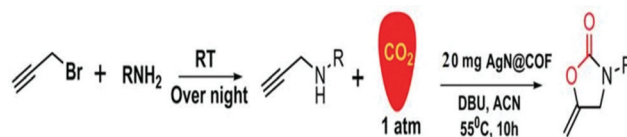
Our group synthesized 2-oxazolidinones from different propargyl amine substrates *via* CO_2 fixation at 55 °C using AgNPs@COF in acetonitrile solvent and using DBU as a base under atmospheric pressure (Scheme 35). We have used benzylamines and propargyl bromide to synthesize propargyl amines, and then CO_2 fixation reactions were performed to obtain

Fig. 22 HRTEM images of the synthesized AgNPs@COF material. Reproduced with permission from ref. 61; copyright: 2020, ChemNanoMat.
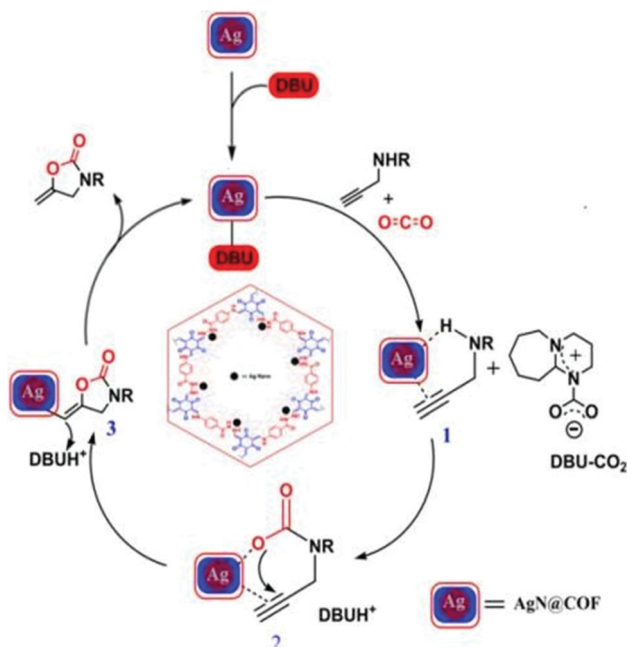

Scheme 35 A general diagram of the synthesis of 2-oxazolidinones. Reproduced with permission from ref. 61; copyright: 2020, ChemNanoMat.

2-oxazolidinones. Before varying the substrate, we optimized several reaction conditions, including the catalyst amount, solvent, base, and reaction temperature. Our research group has shown that the reaction was completed within 10 h with a great 2-oxazolidinone yield of 96%. We have broadly studied substrate variations and yield differentiations. Based on a previous report, a mechanism for 2-oxazolidinone synthesis using AgNPs@COF as a catalyst was proposed, which is presented in Scheme 36.

2-Oxazolidinone synthesis[56] was performed using Ag@TpTta and Ag@TpPa-1 nanocatalysts from propargylic amines and homoallyl amines. Earlier, we discussed the Ag@TpTta and Ag@TpPa-1 nanocatalysts. *Via* using different derivatives of propargylic amine and CO_2 under pressure of 0.1 MPa, we synthesized 2-oxazolidinones under solvent-free conditions with excellent conversion rates (>99%) in a temperature range of 40–80 °C (Scheme 37). Our group gathered information related to the reaction time, temperature, conversion, and yield for both types of COF catalyst and established that the Ag@TpTta catalyst is more proficient for use in the said reaction than the Ag@TpPa-1 catalyst. Our designed catalysts are recyclable for up to five cycles with only negligible changes in catalytic activity.

M. Bhanage *et al.* reported an excellent work on a highly perforated catechol-porphyrin-based COF.[64] In that work, two

Scheme 34 The synthesis of AgNPs@COF. Reproduced with permission from ref. 61; copyright: 2020, ChemNanoMat.

Scheme 36 The reaction mechanism for 2-oxazolidinone synthesis using the synthesized AgNPs@COF material. Reproduced with permission from ref. 61; copyright: 2020, ChemNanoMat.

Scheme 37 The synthesis of 2-oxazolidinones using a AgNP-decorated COF. Reproduced with permission from ref. 56; copyright: 2020, ACS Sustainable Chemistry & Engineering.

covalent organic frameworks (2,3-DhaTph and 2,3-DmaTph) contained super-efficient sites and both acidic (catechol) and basic (porphyrin) moieties. They synthesized 2,3-DhaTph and 2,3-DmaTph COFs following a previously reported process *via* Schiff-base interactions using 2,3-dihydroxyterephthal-aldehyde, 2,3-dimethoxyterephthalaldehyde, and 5,10,15,20-tetrakis(4-aminophenyl)porphin units.[65] They carried out FT-IR, TGA, SEM, BET, and X-ray diffraction analysis to ascertain the properties of the synthesized COFs (Fig. 23). From thermo-gravimetric analysis, it was observed that these COFs have satisfactory surface areas of $\sim$1000 m^2 g^{-1}.

The research group applied these COF-based catalysts to the synthesis of derivatives of oxazolidinone *via* the fixation of CO_2 with aziridines.[66] 1-Methyl-2-phenyl-aziridines were made and used for the formation of 5-aryl-2-oxazolidinones at normal temperature and under 2 MPa pressure using 2,3-DhaTph COF as a catalyst in a solvent-deprived state, as represented in Scheme 38.
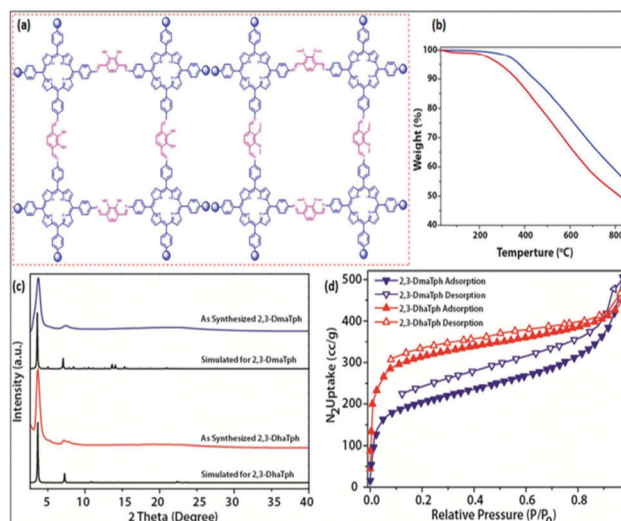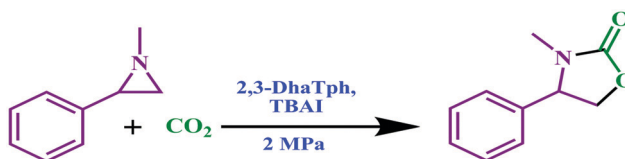

Fig. 23 (a) The structure of a catechol-porphyrin COF; (b) TGA plots of (blue) 2,3-DhaTph and (red) 2,3-DmaTph; (c) PXRD analysis; and (d) N$_2$-BET analysis. Reproduced with permission from ref. 64; copyright: 2016, Catalysis Science & Technology.

Scheme 38 The synthesis of 2-oxazolidinone from aziridine using a 2,3-DhaTph COF.

2.5 Carboxylation of ethynylbenzene

In 2021, En-Qing Gao and his research group reported an excellent Cu(ɪ)-modified covalent organic framework enriched with N–N and N–O chelating groups for the attachment of CO_2 to terminal alkynes.[67] Here, a freshly prepared 2D-COF, named TpBpy, with attached Cu(ɪ) was fabricated from 2,4,6-tri-formylphloroglucinol (Tp) and [2,2′]bipyridinyl-5,5′-diamine (Bpyda), as represented in Scheme 39.[68] Cu(ɪ) was buried inside TpBpy *via* a heterogeneous reaction at ambient temperature in acetonitrile solvent. The concerned COF has an eclipsed and hexagonal structure, which was ascertained based on the XRD pattern. Due to the 2D-structure, the π–π stacking pattern was disturbed when Cu(ɪ) was incorporated. The authors observed a decrease in the crystallinity of the COF after Cu(ɪ) attachment to the COF support.[69] They obtained the interesting observation that the surface area decreases to 434 m^2 per gram from 1480 m^2 per gram when TpBpy was loaded with copper to form TpBpy-Cu-14. TpBpy also showed excellent CO_2 absorption capabilities: 66.8 cm^3 g^{-1} at 0 °C. Also, TpBpy-Cu-14 can absorb 47.2 cm^3 g^{-1} CO_2 at the same temperature. Thermogravimetric analysis helped them to discover that the thermal stability of the COF decreased after metal incorporation. They examined the surface morphology of TpBpy-Cu-14 through SEM analysis and found that the morpho-logy of the COF is unaltered, even after loading with copper(ɪ).

Scheme 39 The structure of TpBpy COF. Reproduced with permission from ref. 67; copyright: 2021, Molecular Catalysis.

Scheme 40 The TpBpy-Cu-COF-based carboxylation of ethynylbenzene.

En-Qing Gao and research team used ethynylbenzene as a sample substrate and let it react with carbon dioxide under atmospheric pressure using TpBpy-Cu-14 as a catalyst (Scheme 40). They studied various control reactions in the presence of the COF (TpBpy-Cu-14) and found that in the presence of Cs_2CO_3, phenylpropionic acid was formed, having yield percentages of 62% and 95% after 6 h and 24 h, respectively, at a controlled temperature of 60 °C. H-Bonding N/O active sites help reactions to occur and activate the terminal alkynes.[70]

In addition to COFs, MOF nanoporous organic polymers are also excellent catalytic materials for the conversion of CO_2 into other valuable products or for the hydrogenation of CO_2. Recently, A. Bhaumik and his research team reported some interesting review articles and research papers regarding this topic in which the use of organic-framework-based catalysts is demonstrated for the hydrogenation and conversion of CO_2.[71]

3. Conclusions and future prospects

In the present era, COFs have become conspicuous materials in the area of catalysis due to their superior CO_2 absorption

capacities. As discussed earlier, metal-incorporating COFs or COFs without metal incorporation can be used effectively in different kinds of CO_2 fixation reactions to obtain valuable organic products. In this review article, we have presented recently synthesized COFs and their applications in different types of CO_2 fixation reactions. COFs are thermally stable compounds with excellent surface areas and pore volumes. In this article, most of the presented COFs are synthesized via Schiff-base mechanisms and are enriched with nitrogen sites. These nitrogen sites can hold and bind CO_2 and different metallic nanoparticles or ions. For this reason, nitrogen-enriched COFs can be used for CO_2 capture and storage and the catalytic fixation of CO_2 with organic substrates. The COFs that are demonstrated show more excellent performance than other conventional catalysts due to their excellent responses towards CO_2. COFs are now being employed for the conversion of CO_2 to CO via photochemical or electrochemical reduction. More research is necessary in this field to develop fruitful applications. This review article will definitely encourage researchers to develop cost-effective COF materials in the near future which can be used for large-scale CO_2 capture. Recently developed COFs should be restructured for the effective capture and binding of CO_2. We hope that this field of research will decrease CO_2 levels in the atmosphere via capturing CO_2 more proficiently.

Conflicts of interest

There are no conflicts to declare.

Acknowledgements

References

1 (a) D. J. Darensbourg and A. D. Yeung, *Polym. Chem.*, 2014, **5**, 3949–3962; (b) A. Appel, J. Bercaw, A. Bocarsly, H. Dobbek, D. DuBois, M. Dupuis, J. Ferry, E. Fujita, R. Hille, P. Kenis, C. Kerfeld, R. Morris, C. Peden, A. Portis, S. Ragsdale, T. Rauchfuss, J. Reek, L. Seefeldt, R. Thauer and G. Waldrop, *Chem. Rev.*, 2013, **113**, 6621–6658.

2 (a) Q. Liu, L. Wu, R. Jackstell and M. Beller, *Nat. Commun.*, 2015, **6**, 5933; (b) M. R. Kember, A. Buchard and C. K. Williams, *Chem. Commun.*, 2011, **47**, 141–163; (c) M. Y. Wang, Y. Cao, X. Liu, N. Wang, L. N. He and S. H. Li, *Green Chem.*, 2017, **19**, 1240–1244; (d) L. Sun, J. H. Ye, W. J. Zhou,

X. Zeng and D. G. Yu, *Org. Lett.*, 2018, **20**, 3049–3052; (*e*) S. S. Islam, P. Bhanja, K. Ghosh, R. A. Molla, N. Yasmin, D. Das and S. M. Islam, *Chem. Select*, 2017, **2**, 10595–10602; (*f*) N. Haque, S. Biswas, S. Ghosh, A. H. Chowdhury, A. Khan and S. M. Islam, *ACS Appl. Nano Mater.*, 2021, **4**, 7663–7674.

3 A. Bar-Even, A. Flamholz, E. Noor and R. Milo, *Biochim. Biophys. Acta*, 2012, **1817**, 1646–1659.

4 (*a*) Y. Zheng, X. Wang, C. Liu, B. Yu, W. Li, H. Wang, T. Sun and J. Jiang, *Inorg. Chem. Front.*, 2021, **8**, 2880–2888; (*b*) I. H. Chowdhury, A. H. Chowdhury, P. Sarkar and S. M. Islam, *ChemNanoMat*, 2021, **7**, 580–591; (*c*) A. H. Chowdhury, I. H. Chowdhury, S. Biswas and S. M. Islam, *Mol. Catal.*, 2020, **493**, 111050; (*d*) A. H. Chowdhury, I. H. Chowdhury and S. M. Islam, *Ind. Eng. Chem. Res.*, 2019, **58**, 11779–11786; (*e*) S. Ghosh, R. A. Molla, U. Kayal, A. Bhaumik and S. M. Islam, *Dalton Trans.*, 2019, **48**, 4657–4666; (*f*) S. M. Islam, D. Mal, B. K. Palit and C. R. Saha, *J. Mol. Catal. A: Chem.*, 1999, **142**, 169–181; (*g*) N. Haque, S. Biswas, P. Basu, I. H. Biswas, R. Khatun, A. Khan and S. M. Islam, *New J. Chem.*, 2020, **44**, 15446–15458; (*h*) A. Sahoo, A. H. Chowdhury, P. Singha, A. Banerjee, S. M. Islam and T. Bala, *Mol. Catal.*, 2020, **493**, 111070; (*i*) P. Bhanja, K. Ghosh, S. S. Islam, A. K. Patra, S. M. Islam and A. Bhaumik, *ACS Sustainable Chem. Eng.*, 2016, **4**(12), 7147–7157; (*j*) S. Roy, P. Bhanja, S. S. Islam, A. Bhaumik and S. M. Islam, *Chem. Commun.*, 2016, **52**, 1871; (*k*) S. Roy, B. Banerjee, A. Bhaumik and S. M. Islam, *RSC Adv.*, 2016, **6**, 31153–31160; (*l*) S. Bhunia, R. A. Molla, V. Kumari, S. M. Islam and A. Bhaumik, *Chem. Commun.*, 2015, **51**, 15732.

5 (*a*) T. K. Pal, D. Deb and P. K. Bharadwaj, *Coord. Chem. Rev.*, 2020, **408**, 213173; (*b*) P. Sarkar, A. H. Chowdhury, S. Riyajuddin, S. Biswas, K. Ghosh and S. M. Islam, *New J. Chem.*, 2020, **44**, 744–752; (*c*) P. Chakrabortty, A. Das, A. H. Chowdhury, S. Ghosh, A. Khan and S. M. Islam, *New J. Chem.*, 2021, **45**, 4738–4745; (*d*) P. Sarkar, A. H. Chowdhury, S. Biswas, A. Khan and S. M. Islam, *Mater. Today Chem.*, 2021, **21**, 100509; (*e*) S. Biswas, R. Khatun, M. Sengupta and S. M. Islam, *Mol. Catal.*, 2018, **452**, 129–137; (*f*) S. Roy, B. Banerjee, A. Bhaumik and S. M. Islam, *RSC Adv.*, 2016, **6**, 31153–31160; (*g*) S. Ghosh, P. Bhanja, R. A. Molla, R. Khatun and S. M. Islam, *Chem. Select*, 2017, **2**, 2159–2165; (*h*) I. H. Chowdhury, A. H. Chowdhury, A. Das, A. Khan and S. M. Islam, *New J. Chem.*, 2020, **44**, 11720–11726; (*i*) P. Sarkar, S. Riyajuddin, A. Das, A. H. Chowdhury, K. Ghosh and S. M. Islam, *Mol. Catal.*, 2020, **484**, 110730; (*j*) S. M. Islam, N. Salam, P. Mondal and A. S. Roy, *J. Mol. Catal A: Chem.*, 2013, **366**, 321–332; (*k*) S. M. Islam, P. Mondal, S. Mukherjee, A. S. Roy and A. Bhaumik, *Polym. Adv. Tech.*, 2011, **22**(6), 933–941; (*l*) M. Sengupta, A. Bag, S. Ghosh, P. Mondal, A. Bordoloi and S. M. Islam, *J. CO₂ Util.*, 2019, **34**, 533–542.

6 (*a*) J. Lu, S. Liu, A. Xu, L. Jin, H. Chi, Y. Li, B. Li, L. Dong and M. Fan, *Mater. Chem. Phys.*, 2021, **272**, 124899; (*b*) R. A. Molla, M. A. Iqubal, K. Ghosh and S. M. Islam, *Green Chem.*, 2016, **18**, 4649–4656; (*c*) R. Khatun, S. Biswas, I. H. Biswas, S. Riyajuddin, N. Haque and K. Ghosh, *J. CO₂ Util.*, 2020, **40**, 101180; (*d*) R. Khatun, P. Bhanja, R. A. Molla, S. Ghosh, A. Bhaumik and S. M. Islam, *Mol. Catal.*, 2017, **434**, 25–31; (*e*) S. Biswas, R. Khatun, M. Dolai, I. H. Biswas, N. Haque, M. Sengupta and S. M. Islam, *New J. Chem.*, 2020, **44**, 141–151; (*f*) I. H. Biswas, S. Biswas, M. S. Islam, S. Riyajuddin, P. Sarkar and K. Ghosh, *New J. Chem.*, 2019, **43**, 14643–14652; (*g*) S. Ghosh, A. Ghosh, S. Riyajuddin, S. Sarkar, A. H. Chowdhury and K. Ghosh, *ChemCatChem*, 2020, **12**, 1055–1067; (*h*) S. Sarkar, S. Ghosh, J. Mondal and S. M. Islam, *Chem. Commun.*, 2020, **56**, 12202–12205; (*i*) T. K. Dey, P. Bhanja, P. Basu, A. Ghosh and S. M. Islam, *Chem. Select*, 2019, **4**, 14315–14328; (*j*) S. Ghosh, A. Ghosh, S. Biswas, M. Sengupta, D. Roy and S. M. Islam, *Chem. Select*, 2019, **4**, 3961–3972; (*k*) S. S. Islam, S. Biswas, R. Ali Molla, N. Yasmin and S. M. Islam, *ChemNanoMat*, 2020, **6**, 1386–1397; (*l*) P. Basu, T. K. Dey, S. Riyajuddin, S. Biswas, K. Ghosh and S. M. Islam, *New J. Chem.*, 2020, **44**, 12680–12691.

7 (*a*) K. Geng, T. He, R. Liu, S. Dalapati, K. T. Tan, Z. Li, S. Tao, Y. Gong, Q. Jiang and D. Jiang, *Chem. Rev.*, 2020, **120**, 8814–8933; (*b*) R. Khatun, S. Biswas, S. Islam, I. H. Biswas, S. Riyajuddin, K. Ghosh and S. M. Islam, *ChemCatChem*, 2019, **11**, 1303–1312; (*c*) M. Sengupta, A. Bag, S. Ghosh, P. Mondal, A. Bordoloi and S. M. Islam, *J. CO₂ Util.*, 2019, **34**, 533–542; (*d*) A. H. Chowdhury, S. Ghosh and S. M. Islam, *New J. Chem.*, 2018, **42**, 14194–14202; (*e*) R. Khatun, P. Bhanja, P. Mondal, A. Bhaumik, D. Das and S. M. Islam, *New J. Chem.*, 2017, **41**, 12937–12946; (*f*) A. H. Chowdhury, U. Kayal, I. H. Chowdhury, S. Ghosh and S. M. Islam, *ChemistrySelect*, 2019, **4**, 1069–1077; (*g*) S. Ghosh, P. Bhanja, N. Salam, R. Khatun, A. Bhaumik and S. M. Islam, *Catal. Today*, 2018, **309**, 253–262; (*h*) R. A. Molla, K. Ghosh, K. Tuhina and S. M. Islam, *New J. Chem.*, 2015, **39**(2), 921–930; (*i*) M. Islam, A. S. Roy and S. Islam, *Catal. Lett.*, 2016, **146**(6), 1128–1138; (*j*) S. M. Islam, N. Salam, P. Mondal, A. S. Roy, K. Ghosh and K. Tuhina, *J. Mol. Catal. A: Chem.*, 2014, **387**, 7–19; (*k*) S. Roy, B. Banerjee, N. Salam, A. Bhaumik and S. M. Islam, *ChemCatChem*, 2015, **7**(17), 2689–2697; (*l*) S. M. Islam, R. A. Molla, A. S. Roy and K. Ghosh, *RSC Adv.*, 2014, **4**(50), 26181–26192; (*m*) S. Roy, T. Chatterjee, B. Banerjee, N. Salam, A. Bhaumik and S. M. Islam, *RSC Adv.*, 2014, **4**(86), 46075–46083; (*n*) S. Ghosh, T. S. Khan, A. Ghosh, A. H. Chowdhury, M. A. Haider and A. Khan, *ACS Sustainable Chem. Eng.*, 2020, **8**(14), 5495–5513; (*o*) R. Khatun, P. Bhanja, P. Mondal, A. Bhaumik, D. Das and S. M. Islam, *New J. Chem.*, 2017, **41**(21), 12937–12946; (*p*) A. H. Chowdhury, S. Ghosh and S. M. Islam, *New J. Chem.*, 2018, **42**(17), 14194–14202.

8 (*a*) B. Gole, V. Stepanenko, S. Rager, M. Grune, D. D. Medina, T. Bein, F. Wurthner and F. Beuerle, *Angew. Chem., Int. Ed.*, 2018, **57**, 846–850; (*b*) T. Sick, A. G. Hufnagel, J. Kampmann, I. Kondofersky, M. Calik, J. M. Rotter, A. Evans, M. Doblinger, S. Herbert, K. Peters, D. Bohm, P. Knochel, D. D. Medina, D. Fattakhova-Rohlfing and T. Bein, *J. Am. Chem. Soc.*, 2018, **140**, 2085–2092; (*c*) X. Zhao,

P. Pachfule and A. Thomas, *Chem. Soc. Rev.*, 2021, **50**, 6871–6913; (*d*) Y. Chen, Q. Chen and Z. Zhang, *Chin. J. Org. Chem.*, 2021, **41**, 3826–3843.

9 (*a*) R. P. Bisbey and W. R. Dichtel, *ACS Cent. Sci.*, 2017, **3**, 533–543; (*b*) N. Huang, P. Wang and D. Jiang, *Nat. Rev. Mater.*, 2016, **1**, 1–19; (*c*) M. S. Lohse and T. Bein, *Adv. Funct. Mater.*, 2018, **28**, 1705553; (*d*) C. S. Diercks and O. M. Yaghi, *Science*, 2017, **355**, eaal1585; (*e*) S. L. Cai, W. G. Zhang, R. N. Zuckermann, Z. T. Li, X. Zhao and Y. Liu, *Adv. Mater.*, 2015, **27**, 5762–5770; (*f*) Y. Song, Q. Sun, B. Aguila and S. Ma, *Adv. Sci.*, 2019, **6**, 1801410; (*g*) I. Omae, *Coord. Chem. Rev.*, 2012, **256**, 1384–1405; (*h*) S. Ghosh, S. Riyajuddin, S. Sarkar, K. Ghosh and S. M. Islam, *ChemNanoMat*, 2020, **6**, 160–172; (*i*) S. Ghosh, P. Mondal, D. Das, K. Tuhina and S. M. Islam, *J. Organomet. Chem.*, 2018, **866**, 1–12; (*j*) N. Salam, P. Paul, S. Ghosh, U. Mandi, A. Khan, S. M. Alam, D. Das and S. M. Islam, *New J. Chem.*, 2020, **44**, 5448–5456; (*k*) S. S. Islam, N. Salam, R. A. Molla, S. Riyajuddin, N. Yasmin, D. Das and K. Ghosh, *Mol. Catal.*, 2019, **477**, 110541; (*l*) R. K. Mondal, S. Riyajuddin, A. Ghosh, S. Ghosh, K. Ghosh and S. M. Islam, *J. Organomet. Chem.*, 2019, **880**, 322–332; (*m*) S. Biswas, D. Roy, S. Ghosh and S. M. Islam, *J. Organomet. Chem.*, 2019, **898**, 120877; (*n*) A. Das, R. K. Mondal, P. Chakrabortty, S. Riyajuddin and A. H. Chowdhury, *Mol. Catal.*, 2021, **499**, 111253.

10 A. P. Cote, A. I. Benin, N. W. Ockwig, M. O'Keeffe, A. J. Matzgerand and O. M. Yaghi, *Science*, 2005, **310**, 1166–1170.

11 (*a*) P. J. Waller, Y. S. AlFaraj, C. S. Diercks, N. N. Jarenwattananon and O. M. Yaghi, *J. Am. Chem. Soc.*, 2018, **140**, 9099–9103; (*b*) T. Ma, E. A. Kapustin, S. X. Yin, L. Liang, Z. Zhou, J. Niu, L.-H. Li, Y. Wang, J. Su, J. Li, X. Wang, W. D. Wang, W. Wang, J. Sun and O. M. Yaghi, *Science*, 2018, **361**, 48–52.

12 S. Y. Ding and W. Wang, *Chem. Soc. Rev.*, 2013, **42**, 548–568.

13 S. Dey, A. Bhunia, D. Esquivel and C. Janiak, *J. Mater. Chem. A*, 2016, **4**, 6259–6263.

14 F. Haase, E. Troschke, G. Savasci, T. Banerjee, V. Duppel, S. Dorfler, M. M. J. Grundei, A. M. Burow, C. Ochsenfeld, S. Kaskel and B. V. Lotsch, *Nat. Commun.*, 2018, **9**, 2600.

15 L. Stegbauer, K. Schwinghammer and B. V. Lotsch, *Chem. Sci.*, 2014, **5**, 2789–2793.

16 C. R. DeBlase, K. E. Silberstein, T. T. Truong, H. D. Abruna and W. R. Dichtel, *J. Am. Chem. Soc.*, 2013, **135**, 16821–16824.

17 L. Zhai, N. Huang, H. Xu, Q. Chen and D. Jiang, *Chem. Commun.*, 2017, **53**, 4242–4245.

18 B. Dong, L. Wang, S. Zhao, R. Ge, X. Song, Y. Wang and Y. Gao, *Chem. Commun.*, 2016, **52**, 7082–7085.

19 S. Zhao, B. Dong, R. Ge, C. Wang, X. Song, W. Ma, Y. Wang, C. Hao, X. Guo and Y. Gao, *RSC Adv.*, 2016, **6**, 38774–38781.

20 N. Huang, X. Chen, R. Krishna and D. Jiang, *Angew. Chem., Int. Ed.*, 2015, **54**, 2986–2990.

21 D. Chakraborty, P. Shekhar, H. D. Singh, R. Kushwaha, C. P. Vinod and R. Vaidhyanathan, *Chem. – Asian J.*, 2019, **14**, 4767–4773.

22 H. He, Q. Q. Zhu, W. W. Zhang, H. W. Zhang, J. Chen, C. P. Li and M. Du, *ChemCatChem*, 2020, **12**, 5192–5199.

23 K. Xu, Y. Dai, B. Ye and H. Wang, *Dalton Trans.*, 2017, **46**, 10780–10785.

24 A. Chen, Y. Zhang, J. Chen, L. Chen and Y. Yu, *J. Mater. Chem. A*, 2015, **3**, 9807–9816.

25 Y. Zhi, P. Shao, X. Feng, H. Xia, Y. Zhang, Z. Shi and X. Liu, *J. Mater. Chem. A*, 2018, **6**, 374–382.

26 M. Sengupta, A. Bag, S. Ghosh, P. Mondal, A. Bordoloi and S. M. Islam, *J. CO$_2$ Util.*, 2019, **34**, 533–542.

27 S. Karak, S. Kandambeth, B. P. Biswal, H. S. Sasmal, S. Kumar, P. Pachfule and R. Banerjee, *J. Am. Chem. Soc.*, 2017, **139**, 1856–1862.

28 Y. Han, M. Zhang, Y. Q. Zhang and Z. H. Zhang, *Green Chem.*, 2018, **20**, 4891–4900.

29 P. Guan, J. Qiu, Y. Zhao, H. Wang, Z. Li, Y. Shi and J. Wang, *Chem. Commun.*, 2019, **55**, 12459–12462.

30 (*a*) D. M. Fischbach, G. Rhoades, C. Espy, F. Goldberg and B. J. Smith, *Chem. Commun.*, 2019, **55**, 3594–3597; (*b*) T. Ma, E. A. Kapustin, S. X. Yin, L. Liang, Z. Zhou, J. Niu, L. Li, Y. Wang, J. Su, J. Li, X. Wang, W. D. Wang, W. Wang, J. Sun and O. M. Yaghi, *Science*, 2018, **361**, 48–52; (*c*) C. Wang, Y. Wang, R. Ge, X. Song, X. Xing, Q. Jiang, H. Lu, C. Hao, X. Guo, Y. Hao and D. Jiang, *Chem. – Eur. J.*, 2018, **24**, 585–589; (*d*) Q. Lu, Y. Ma, H. Li, X. Guan, Y. Yusran, M. Xue, Q. Fang, Y. Yan, S. Qiu and V. Valtchev, *Angew. Chem., Int. Ed.*, 2018, **57**, 6042–6048; (*e*) R. Mercado, R.-S. Fu, A. V. Yakutovich, L. Talirz, M. Haranczyk and B. Smit, *Chem. Mater.*, 2018, **30**, 5069–5086; (*f*) X. Han, J. Huang, C. Yuan, Y. Liu and Y. Cui, *J. Am. Chem. Soc.*, 2018, **140**, 892–895.

31 (*a*) R. Mercado, R. S. Fu, A. V. Yakutovich, L. Talirz, M. Haranczyk and B. Smit, *Chem. Mater.*, 2018, **30**, 5069–5086; (*b*) H. Furukawa and O. M. Yaghi, *J. Am. Chem. Soc.*, 2009, **131**, 8875–8883; (*c*) L. A. Baldwin, J. W. Crowe, D. A. Pyles and P. L. McGrier, *J. Am. Chem. Soc.*, 2016, **138**, 15134–15137.

32 L. G. Ding, B. J. Yao, F. Li, S. C. Shi, N. Huang, H. B. Yin, Q. Guan and Y. B. Dong, *J. Mater. Chem. A*, 2019, **7**, 4689–4698.

33 F. Li, L. G. Ding, B. J. Yao, N. Huang, J. T. Li, Q. J. Fu and Y. B. Dong, *J. Mater. Chem. A*, 2018, **6**, 11140–11146.

34 C. Müller, D. Rahmat, F. Sarti, K. A. Leithner and B. Schnürch, *J. Mater. Chem. A*, 2012, **22**, 3899–3908.

35 B. J. Yao, L. G. Ding, F. Li, J. T. Li, Q. J. Fu, Y. J. Ban, A. Guo and Y. B. Dong, *ACS Appl. Mater. Interfaces*, 2017, **9**, 38919–38930.

36 Y. Zhao, Y. Zhao, J. Qiu, Z. Li, H. Wang and J. Wang, *ACS Sustainable Chem. Eng.*, 2020, **8**, 18413–18419.

37 K. Jeong, S. Park, G. Jung, S. Kim, Y. Lee, S. Kwak and S. Lee, *J. Am. Chem. Soc.*, 2019, **141**, 5880–5885.

38 J. Qiu, Y. Zhao, Z. Li, H. Wang, Y. Shi and J. Wang, *ChemSusChem*, 2019, **12**, 2421–2427.

39 F. Yang, Y. Li, T. Zhang, Z. Zhao, G. Xing and L. Chen, *Chem. – Eur. J.*, 2020, **26**, 4510–4514.

40 H. Zhong, J. Gao, R. Sa, S. Yang, Z. Wu and R. Wang, *ChemSusChem*, 2020, **13**, 6323–6329.

41 (a) S. Wang and C. Xi, *Chem. Soc. Rev.*, 2019, **48**, 382–404; (b) X. Sun, L. Lu, Q. Zhu, C. Wu, D. Yang, C. Chen and B. Han, *Angew. Chem., Int. Ed.*, 2018, **57**, 2427–2431; (c) J. Qiu, Y. Zhao, Z. Li, H. Wang, M. Fan and J. Wang, *ChemSusChem*, 2017, **10**, 1120–1127; (d) F. D. Bobbink, W. Zhong, Z. Fei and P. J. Dyson, *ChemSusChem*, 2017, **10**, 2728–2735.

42 (a) S. Jayakumar, H. Li, Y. Zhao, J. Chen and Q. Yang, *Chem. – Asian J.*, 2017, **12**, 577–585; (b) W. Zhang, F. Ma, L. Ma, Y. Zhou and J. Wang, *ChemSusChem*, 2020, **13**, 341–350; (c) M. B. Sogo, H. Garciab and C. Aprile, *Catal. Sci. Technol.*, 2015, **5**, 1222–1230.

43 S. Haldar, K. Roy, S. Nandi, D. Chakraborty, D. Puthusseri, Y. Gawli, S. Ogale and R. Vaidhyanathan, *Adv. Energy Mater.*, 2018, **8**, 1702170.

44 W. Zhou, Q. W. Deng, G. Q. Ren, L. Sun, L. Yang, Y. M. Li and W. Q. Deng, *Nat. Commun.*, 2020, **11**, 4481.

45 Y. Xie, T. T. Wang, X. H. Liu, K. Zou and W. Q. Deng, *Nat. Commun.*, 2013, **4**, 1960.

46 Y. Zhang, H. Hu, J. Ju, Q. Yan, V. Arumugam, X. Jing and Y. Gao, *Chin. J. Catal.*, 2020, **41**, 485–493.

47 (a) J. Sun, S. Zhang, W. Cheng and J. Ren, *Tetrahedron Lett.*, 2008, **49**, 3588–3591; (b) V. Caló, A. Nacci, A. Monopoli and A. Fanizzi, *Org. Lett.*, 2002, **4**, 2561–2563.

48 J. M. Sun, S. Fujita and M. Arai, *J. Organomet. Chem.*, 2005, **690**, 3490–3497.

49 (a) J. Peng and Y. Deng, *New J. Chem.*, 2001, **25**, 639–641; (b) H. Kawanami, A. Sasaki, K. Matsui and Y. Ikushima, *Chem. Commun.*, 2003, 896–897.

50 H. Yang, Y. Gu, Y. Deng and F. Shi, *Chem. Commun.*, 2002, 274–275.

51 P. Sarkar, S. Riyajuddin, A. Das, A. H. Chowdhury, K. Ghosh and S. M. Islam, *Mol. Catal.*, 2020, **484**, 110730.

52 P. Sarkar, A. H. Chowdhury, S. Riyajuddin, S. Biswas, K. Ghosh and S. M. Islam, *New J. Chem.*, 2020, **44**, 744–752.

53 S. Karak, S. Kandambeth, B. P. Biswal, H. Sekhar Sasmal, S. Kumar, P. Pachfule and R. Banerjee, *J. Am. Chem. Soc.*, 2017, **139**, 1856–1862.

54 A. H. Chowdhury, I. H. Chowdhury, S. Biswas and S. M. Islam, *Mol. Catal.*, 2020, **493**, 111050.

55 X. Ding, J. Guo, X. Feng, Y. Honsho, J. Guo, S. Seki, P. Maitarad, A. Saeki, S. Nagase and D. Jiang, *Angew. Chem., Int. Ed.*, 2011, **50**, 1289–1293.

56 S. Ghosh, T. S. Khan, A. Ghosh, A. H. Chowdhury, M. A. Haider, A. Khan and S. M. Islam, *ACS Sustainable Chem. Eng.*, 2020, **8**, 5495–5513.

57 S. Karak, S. Kandambeth, B. P. Biswal, H. S. Sasmal, S. Kumar, P. Pachfule and R. Banerjee, *J. Am. Chem. Soc.*, 2017, **139**, 1856–1862.

58 R. Khatun, S. Biswas, I. H. Biswas, S. Riyajuddin, N. Haque, K. Ghosh and S. M. Islam, *J. CO$_2$ Util.*, 2020, **40**, 101180.

59 S. Chandra, D. R. Chowdhury, M. Addicoat, T. Heine, A. Paul and R. Banerjee, *Chem. Mater.*, 2017, **29**, 2074–2080.

60 P. Puthiaraj and W. S. Ahn, *Catal. Sci. Technol.*, 2016, **6**, 1701–11709.

61 S. S. Islam, S. Biswas, Dr. R. Ali Molla, Dr. N. Yasmin and S. M. Islam, *ChemNanoMet*, 2020, **6**, 1386–1397.

62 (a) S. Karak, S. Kandambeth, B. P. Biswal, H. S. Sasmal, S. Kumar, P. Pachfule and R. Banerjee, *J. Am. Chem. Soc.*, 2017, **139**, 1856–1862; (b) L. Wang, C. Zeng, H. Xu, P. Yin, D. Chen, J. Deng, M. Li, N. Zheng, C. Gu and Y. Ma, *Chem. Sci.*, 2019, **10**, 1023–1028; (c) S. Ghosh, R. A. Molla, U. Kayal, A. Bhaumik and S. M. Islam, *Dalton Trans.*, 2019, **48**, 4657–4666; (d) M. Sengupta, A. Bag, S. Ghosh, P. Mondal, A. Bordoloi and S. M. Islam, *J. CO2 Util.*, 2019, **34**, 533–542; (e) N. Haque, S. Biswas, S. Ghosh, A. H. Chowdhury, A. Khan and S. M. Islam, *ACS Appl. Nano Mater.*, 2021, **4**, 7663–7674; (f) S. Ghosh, R. A. Molla, U. Kayal, A. Bhaumik and S. M. Islam, *Dalton Trans.*, 2019, **48**, 4657–4666.

63 (a) Y. Wu, Z. Wang, S. Chen, J. Wu, X. Guo and Z. Liu, *RSC Adv.*, 2015, **5**, 87151–87156; (b) S. Li, Y. Shen, A. Xie, X. Yu, L. Qiu, L. Zhang and Q. Zhang, *Green Chem.*, 2007, **9**, 852–858.

64 V. Saptal, D. B. Shinde, R. Banerjee and B. M. Bhanage, *Catal. Sci. Technol.*, 2016, **6**, 6152–6158.

65 D. B. Shinde, S. Kandambeth, P. Pachfule, R. Kumar and R. Banerjee, *Chem. Commun.*, 2015, **51**, 310–313.

66 (a) R. Watson, D. Batty, A. Baxter, D. Hannah, D. Owen and J. Montana, *Tetrahedron Lett.*, 2002, **43**, 683–685; (b) L. Aurelio, R. Brownlee and A. Hughes, *Chem. Rev.*, 2004, **104**, 5823–5846; (c) T. Mukhtar and G. Wright, *Chem. Rev.*, 2005, **105**, 529–542; (d) T. Andreou, A. Costa, L. Esteban, L. Gonzalez, G. Mas and J. Vilarrasa, *Org. Lett.*, 2005, **7**, 4083–4086; (e) R. Watile, D. Bagal, K. Deshmukh, K. Dhake and B. M. Bhanage, *J. Mol. Catal. A: Chem.*, 2011, **351**, 196–203; (f) Y. N. Zhao, Z. Z. Yang, S. H. Luo and L. N. He, *Catal. Today*, 2013, **200**, 2–8.

67 R. Bu, L. Zhang, L. L. Gao, W. J. Sun, S. L. Yang and E. Q. Gao, *Mol. Catal.*, 2021, **499**, 111319.

68 W. Zhong, R. Sa, L. Li, Y. He, L. Li, J. Bi, Z. Zhuang, Y. Yu and Z. Zou, *J. Am. Chem. Soc.*, 2019, **141**, 7615–7621.

69 D. Wu, Q. Xu, J. Qian, X. Li and Y. Sun, *Chem. – Eur. J.*, 2019, **25**, 3105–3111.

70 (a) X. Lan, C. Du, L. Cao, T. She, Y. Li and G. Bai, *ACS Appl. Mater. Interfaces*, 2018, **10**, 38953–38962; (b) W. Zhang, Y. Mei, X. Huang, P. Wu, H. Wu and M. He, *ACS Appl. Mater. Interfaces*, 2019, **11**, 44241–44248; (c) M. Ding, R. W. Flaig, H. L. Jiang and O. M. Yaghi, *Chem. Soc. Rev.*, 2019, **48**, 2783–2828.

71 (a) A. Modak, A. Ghosh, A. Bhaumik and B. Chowdhury, *Adv. Colloid Interface Sci.*, 2021, **290**, 102349; (b) S. K. Das, A. Ghosh, S. Bhattacharjee, A. Chowdhury, P. Mitra and A. Bhaumik, *New J. Chem.*, 2021, **45**, 9189–9196; (c) A. Modak, A. Ghosh, A. R. Mankar, A. Pandey, M. Selvaraj, K. K. Pant, B. Chowdhury and A. Bhaumik, *ACS Sustainable Chem. Eng.*, 2021, **9**(37), 12431–12460.